DEVELOPMENT AND ON-LINE TESTS OF DIFFERENT TARGET-ION SOURCE UNITS FOR PRODUCTION OF NUCLIDES FAR FROM STABILITY

V.N. Panteleev, A.E. Barzakh, D.V. Fedorov, A.M. Ionan, V.S. Ivanov, K.A. Mezilev, P.L. Molkanov, F.V. Moroz, S.Yu. Orlov, Yu.M. Volkov

1. Introduction

The work carried out has as a general goal the development of a massive (up to 1 kg) uranium carbide target prototype for the third generation ISOL facilities, where two-step reactions will be used to produce intense neutron-rich nuclear beams.

For more than thirty years UC_x targets have been explored for the production of a large set of neutron-rich and neutron-deficient heavy nuclei. The main line of uranium carbide target development was the creation of the target material with a high dispersivity and porosity in order to decrease the release time of the species produced by different reactions in the target material, which is mainly determined by the diffusion and effusion processes. On the other hand, for a more efficient use of a neutron beam after the primary beam converter the density of the target material containing uranium should be as high as possible. Additionally, the target material with a higher density has a higher thermal conductivity that would allow dissipating a higher power introduced into the target by the primary beam, when the target is used for exotic nuclei production in the direct reaction. Hence, for more effective production of short-lived isotopes of the element chosen for the investigation, a special selection of a metal carbide target material is required – concerning not only the target material structure but also its density. At the IRIS (Investigation of Radioactive Isotopes at Synchrocyclotron) facility in Gatchina uranium carbide target materials of different structure and density have been tested.

The first general goal of the work is to find out whether the high density uranium carbide can be competitive with presently used low density UC_x targets in the production of short-lived nuclei far from stability. The yields and release characteristics are reported here to compare properties of tested target materials. The second goal is the development and tests of an effective, high-temperature target unit for the on-line production of short-lived rare nuclides. The peculiarity of the developed target unit is the absence of the ion source [1]. The ionization process happens in the target volume itself, so it can help to avoid an additional delay time due to the effusion inside the transfer tube and the ion source. The combined target-ion source (CTIS) unit could be especially useful for the production of isotopes of hard volatile elements with long sticking time, such as rare-earth elements Gd and Lu, and of many other nuclides with boiling points higher than 3000°C. The use of tungsten container [2] instead of a traditional tantalum one allowed to rise the target working temperature up to 2500°C, thereby decreasing the delay time for nuclides produced in the target and hence increasing the yield of short-lived isotopes. At the same time, a high work function of tungsten ensures a high efficiency of a surface ionization of the species with the ionization potentials lower than 6 eV produced in the target material.

2. Target materials tested on-line

A schematic view of the typical target unit used for different uranium carbide target material tests is shown in Fig. 1. As a first step in that comparison, the isotopes of alkali elements Rb, Cs and Fr have been selected for the yield and release efficiency measurements. The main reason of such a choice was their high ionization efficiency (theoretically up to 100%) on the hot inner surface of the target-ion source unit, that allows to obtain short-lived nuclei far from stability. This is very important for the target material comparison.

The second important point in the selection of alkalis is that the target construction can be very simple, including only the tungsten target cavity (ionizing target) [3], as the ionization process happens inside the target container itself. It allows to avoid some uncertainties concerning possible temperature difference of the tested units, as in that case only one parameter (the target container temperature) should be controlled in the course of the experiment.

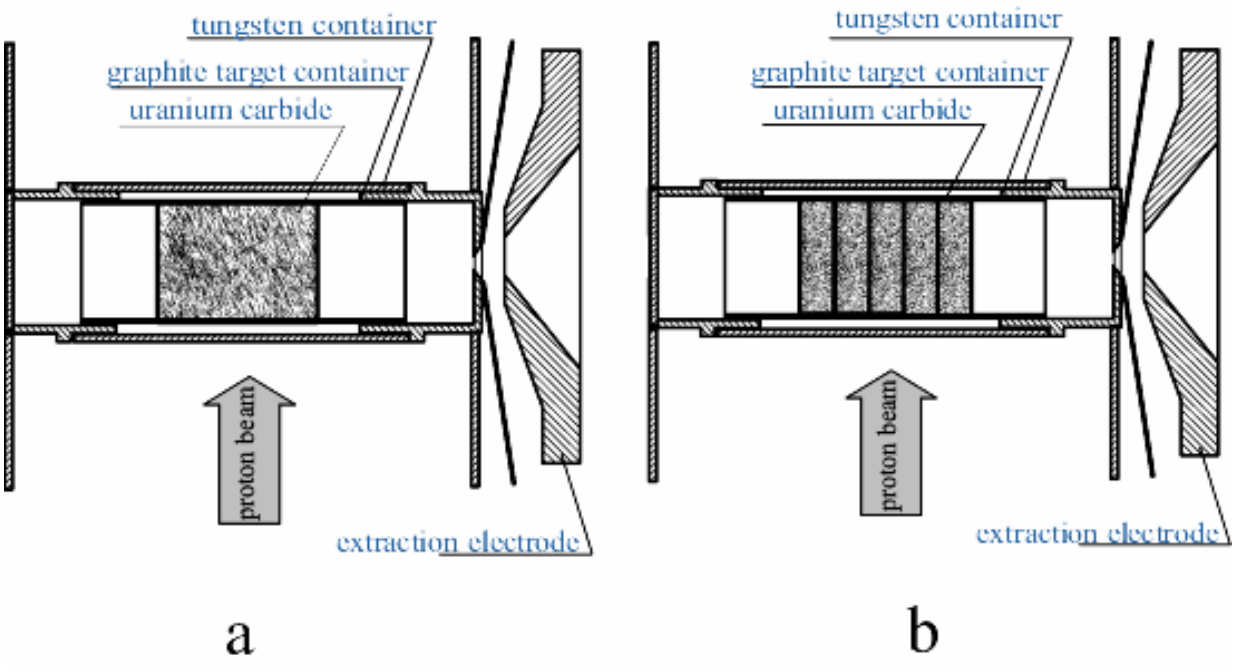

Fig. 1. Schematic drawings of a) high density rod (HDR) uranium carbide target; b) high and low density pellet uranium carbide target

Three kinds of the target materials were studied: a high density UC rod; a low density UC_x target prepared by the ISOLDE method at the IRIS facility (as few pellets placed transversely to the axis of the target); a high density UC powder target material prepared by the method of the powder metallurgy. The high density rod (HDR) target had the following characteristics: uranium rod density 11 g/cm^3, target thickness 6.7 g/cm^2, about 6 mm length and 11 mm in diameter. The grain size was about 200 μm. The low density target (LDT) had: uranium density 2.3 g/cm^3, target thickness 2.8 g/cm^2, about 12 mm length and 11 mm in diameter; 8 pellets, each of 1.2–1.6 mm thickness with the grain size about 20 μm. This target material has been prepared by the Orsay–PNPI collaboration at the IRIS facility, using the ISOLDE technology, a similar graphite powder brought by Orsay group and uranium dioxide from Russian producers. This target is also referred later as ISOLDE like or PARRNe-IRIS. The high density powder (HDP) target had: uranium density 12 g/cm^3, target thickness 6.3 g/cm^2, length 5.25 mm, diameter 11.2 mm; 3 pellets, each of 1.6–1.9 mm thickness, grain size about 20 μm. Targets were operated in the temperature range of 1900–2200°C. The investigated target materials were maintained in the target containers of the same dimensions and geometry. More detailed description of used target construction can be found in Refs. [4, 5]. The uranium fission reaction was produced by 1 GeV proton beam with the intensity of 50–70 nA. Mass-separated isotope beams were collected on a tape station and were either transported to γ-, β-, α-counting stations or directly counted by α-detector to be identified by the characteristic lines. Detailed description of γ-rays measurement and yield determination can be found in Ref. [4]. The yields of Cs isotopes were determined by means of β-counter as well as of γ-detector. Fr isotopes were produced in the same targets by the spallation reaction. The Fr isotope yields were measured using γ-rays and α-particles. To get consistent yield data obtained by α- and γ-measurements, the α-yield data were normalized to the yields obtained by γ-measurement (as the efficiency of the Ge detector is well known), taking as normalizing coefficient the yield ratio for isotopes measured by both methods.

2.1. Yield comparison

For the investigated target materials the Cs and Fr yields under similar temperature conditions (T = 2100°C) have been determined. All presented yield values were normalized to a target thickness of 1 g/cm^2 and 0.1 μA proton beam current. The error of the temperature measurement for different targets can reach 50°C. The experimental errors of the obtained yield values are within the limits of 30% for isotopes not far from stability and of 80% for short-lived neutron-rich isotopes. Cs yields from the investigated targets are plotted together with the ISOLDE yields obtained for standard target at the PS-Booster and for graphite cloth target at the synchrocyclotron. As one can see in Fig. 2, there is a good agreement of yields from similar target materials of ISOLDE and PARRNe-IRIS. The yields of short-lived Cs isotopes from a HDR target are 1.5–2 times lower. This fact demonstrates its lower release efficiency than the ISOLDE or PARRNe-IRIS target. It is an expected result, as the grain size of the HDR target is 10 times larger. Therefore the diffusion process should be much slower. The yields measured for Rb isotopes, which are not presented here, confirm the results obtained for Cs. The Cs yield trend from the lately developed HDP pellet target is similar to the fast PARRNe-IRIS target, but the efficiency is about 20 times less. It can be explained by a strong carbonization of the inner surface of the target container that leads to the ionization efficiency decrease, as the HDP target had been outgased much longer time than other targets. The calculated yields based on the experimental cross sections are also presented to show the in-target production rate of the investigated isotopes. The enhancement of the yield of ^{139}Cs from the HDR target respectively to the calculated one can be explained by the decay of the mother ^{139}Xe nucleus that has the production cross section comparable to the Cs daughter nucleus. It is worth stressing that the yield excess in respect to the calculated yield values was measured only for Cs isotopes produced from the HDR target. It can indicate that in the HDR target the Xe precursors may have longer release times, therefore allowing a large probability of decay in the target as an additional production mode. That assumption requires a special verification.

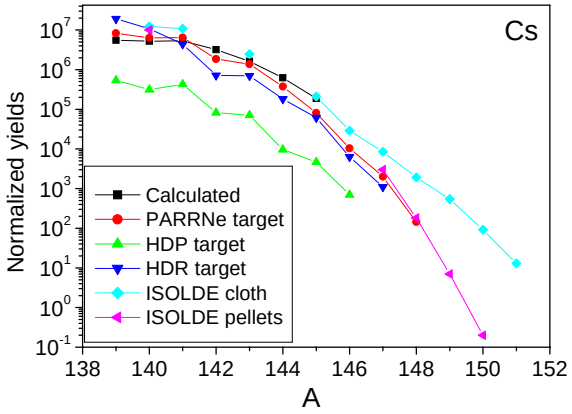

Fig. 2. The yields of Cs isotopes released from a high density rod, high density and low density pellet targets at 2100°C. The yields from ISOLDE UC_x pellet target are presented. The yields calculated on the basis of measured cross section are shown as well

It should be specially pointed out the extraordinary high yields of short-lived Rb and Cs obtained from the ISOLDE graphite cloth UC_x target at the SC. Unfortunately, these high yield data were not reproduced at the PS-Booster, where presently the ISOLDE standard powder-pellet UC_x target is used.

In Fig. 3 the yields of Fr isotopes from the HDR and HDP targets are presented. Fr isotopes have not been measured from PARRNE-IRIS target. The yields of short-lived ^{214}Fr ($T_{1/2}$ = 5 ms), ^{218}Fr ($T_{1/2}$ = 1 ms) and ^{219}Fr ($T_{1/2}$ = 21 ms) were measured by detection their characteristic α-decays. The yields of isotopes with longer half-

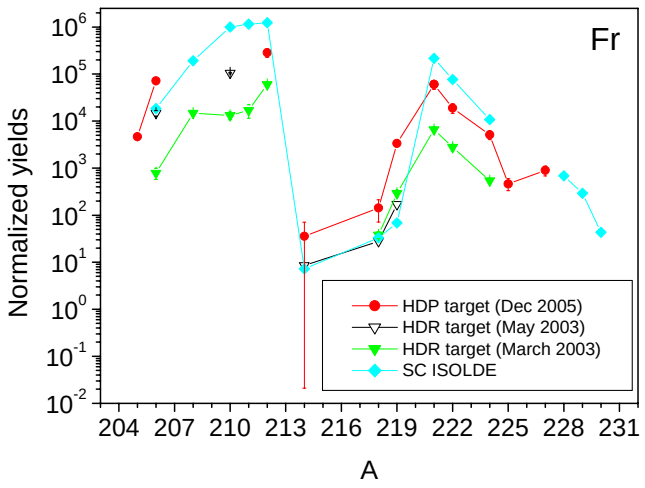

Fig. 3. The yields of Fr isotopes from the HDR, HDP and ISOLDE graphite-cloth targets

lives were determined using both α-particles and γ-rays. The Fr isotope yields obtained at the ISOLDE from the UC_x graphite-cloth target are also shown in the graph. The normalized yields of long-lived Fr isotopes from the ISOLDE graphite-cloth target are higher than from the HDR and HDP targets. The lower HDR and HDP target efficiency, which is the product of the ionization and release efficiencies, may be explained by lower value of the ionization efficiency of the ionizing targets used for experiments, where the ionization process takes place on the strongly carbonized inner surface of the target container. But, at the same time, the normalized yields of short-lived $^{214, 218, 219}$Fr are equal or even higher than the yields of these short-lived isotopes from the ISOLDE target. As there was only one measurement of the Fr yields from a newly developed HDP target, we give here the obtained yield values from that target as preliminary ones.

2.2. Comparison of the target release properties

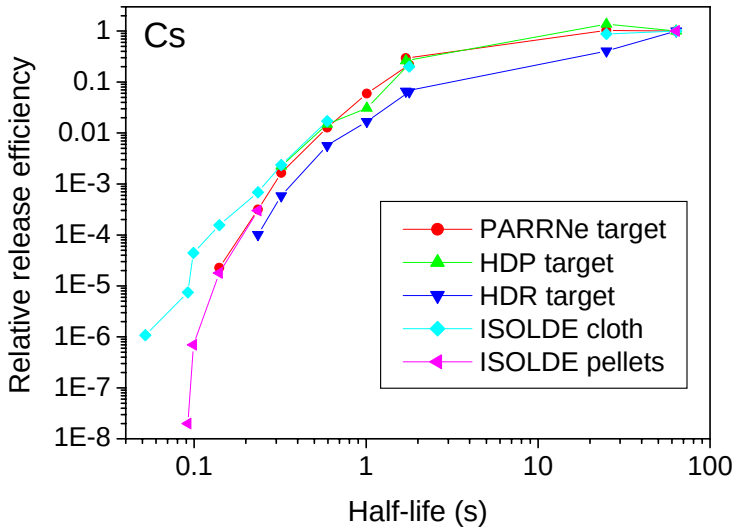

Fig. 4. Comparison of the Cs yield trends from HDR, HDP, LDP PARRNe IRIS and ISOLDE targets. The yields are normalized at the yield point of ^{140}Cs with the half-life $T_{1/2}$ = 63.7 s

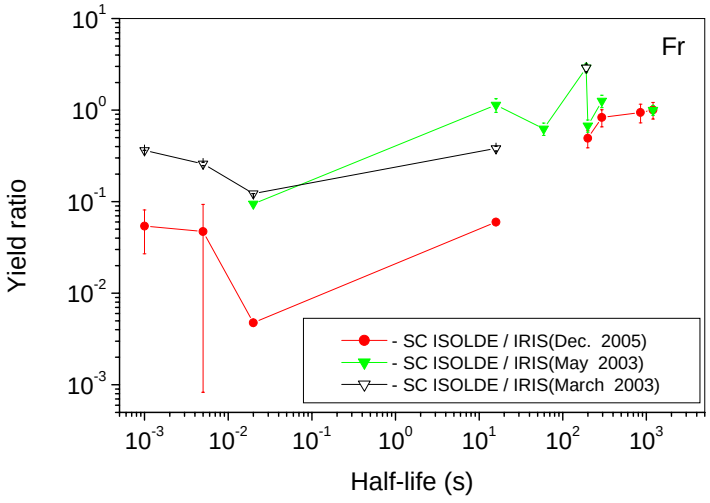

Fig. 5. Ratio of the yields of Fr isotopes from ISOLDE graphite-cloth target to the yields of the same isotopes from HDR (triangles) and HDP (circles) targets, plotted as a function of the half-lives. The obtained ratios are normalized at the point ^{212}Fr with the half-life $T_{1/2}$ = 20 min

The comparison of the relative release efficiencies of different targets for produced isotopes has been derived by normalizing the obtained yield values to the yield of a long-lived isotope ^{140}Cs ($T_{1/2}$ = 63.7 s) which is produced with the efficiency close to unity. In Fig. 4 the relative release efficiencies of Cs isotopes are presented as functions of their half-lives. The trend of the normalized yield values demonstrates that the ISOLDE and PARRNe-IRIS targets in general are slightly faster than the HDR target. A rather promising result is that the trend of the relative efficiency curve for the newly developed HDP target coincidences with one of the ISOLDE target.

For comparison of the Fr release efficiencies, the yields from the ISOLDE cloth target were divided by the measured yields of the same isotopes from the HDR and HDP targets and normalized to the yield ratio of ^{212}Fr. The obtained ratio values are shown in Fig. 5 as functions of the half-lives; as the Fr isotopes were not studied with the PARRNe target, only the ratios for the HDR and HDP targets are presented. The result for the HDP target is preliminary. As one can see, the HDR and HDP targets has considerably higher release efficiency for short lived-isotopes of ^{214}Fr ($T_{1/2}$ = 5 ms), ^{218}Fr ($T_{1/2}$ = 1 ms) and ^{219}Fr ($T_{1/2}$ = 21 ms). This can be explained by the fact that the sticking and flight time of species produced in the IRIS tested target prototypes is about six time less than in the ISOLDE target due to the ratio of the volumes of the target containers. To confirm or to reject the

assumption of a much shorter effusion time some additional on-line tests on the short-lived Fr isotope production from a HDP target will be carried out at the IRIS facility.

3. Ionizing targets for production of nuclides with high ionization potentials

For the production of nuclides with high ionization potentials three types of combined targets have been developed and on-line tested:

1. The ionizing foil target of the surface ionization for the Li and rare-earth isotope production.
2. The laser foil target for the production and resonance laser spectroscopy investigation of neutron-deficient rare-earth isotopes.
3. The combined target-ion source unit of the electron beam ionization with uranium carbide as a target material for the production of neutron-rich isotopes of the elements with the ionization potentials higher than 6 eV.

3.1. Off-line measurements of the ionization efficiencies for Li, Sm, Eu, Tm, and Yb

The schematic diagram shows the high-temperature ionizing target [6] used for on-line tests (Fig. 6). The only difference in the construction of the ionizing target (IT) used for off-line ionization efficiency measurements was the presence of a separately heated oven which was connected to the IT for a slow evaporation of the sample consisting of a known amount of atoms of the element being investigated.

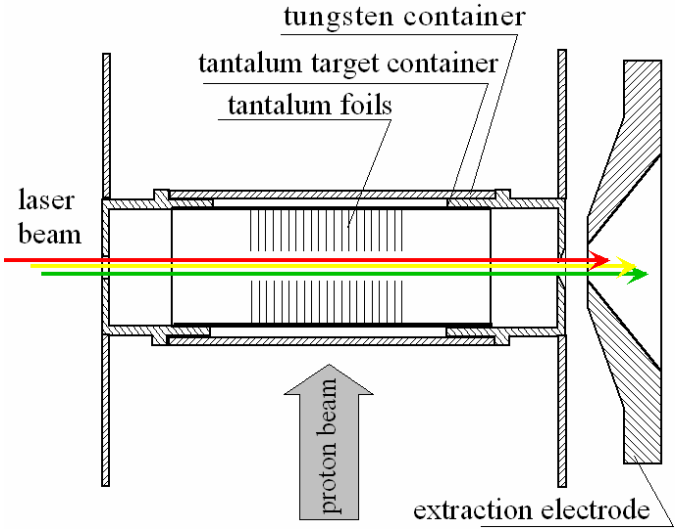

Fig. 6. Scheme of the combined target-ion source unit for Li, rare-earth isotope production and laser spectroscopy experiments

Off-line measurements of the surface ionization efficiencies for Li and rare-earth elements was carried out by using samples of LiF and oxides of pointed out rare-earth elements weighting from 10 to 20 μg placed into the oven connected with the IT volume. The current of each evaporated sample was measured by a Faraday cup placed in the focal plane of the mass-separator magnet and connected with the current integrator. The process of the laser ionization efficiency measurement of Eu and Gd atoms inside the target volume was carried out simultaneously with the surface ionization measurement. For that purpose three laser beams tuned in resonance with appropriate transitions in Eu and Gd were introduced into the CTIS. We indicate this method as the laser target (LT) [7], in order to emphasize that it differs from the method employing the resonance ionization in the laser ion source (LIS) [8].

Table 1

The efficiencies of ionization measured off-line with IT and LT

Element	Temperature, °C	Surface ionization efficiency, %	Laser ionization efficiency, %
Li	2000	6	
Rb	2000	40	
Cs	2000	55	
Sm	2200	7	
Eu	2200	10	7
Gd	2500	2	1
Tm	2200	3	
Yb	2200	5	

In Table 1 the efficiencies of surface and laser ionization measured off-line for some alkalis and rare-earth elements are presented. The error of the ionization efficiency measurements was 20% for Rb and Cs and up to 40% for other elements.

3.2. On-line measurements of the yield of neutron-deficient rare-earth isotopes

A 1 GeV proton beam induced spallation reactions in the target material (tantalum foils, target thickness 3 g/cm^2) producing nuclides of neutron-deficient isotopes of rare-earth elements. After surface or laser ionization and extraction from the target, the ions were separated by a mass-separator and implanted into a moving tape installed at one of the three beam-lines of the IRIS facility. An identification of the radioactive implanted specimens and yield determination were performed by means of appropriate γ-line measurements by a coaxial high-purity germanium detector. The proton beam intensity was 0.05 μA. In Table 2 the yields of the neutron-deficient rare-earth isotopes produced on-line, the yields calculated by the EPAX code and the values of the efficiency of the ionizing target are presented.

Table 2

On-line yields and production efficiencies of the IT at 2500°C

Nuclide	$T_{1/2}$	Yields measured, s^{-1}	Yields EPAX, s^{-1}	Production efficiency by surface ionization, %	Production efficiency by laser ionization, %
^{138}Eu	12.1 s	2.4×10^3	9.5×10^4		
^{139}Eu	17.9 s	1.6×10^4	4.9×10^5		
^{141}Eu	41.4 s	4.0×10^5	5.6×10^6		
^{142}Eu	1.22 min	4.1×10^5	1.2×10^7		
^{143}Eu	2.57 min	2.0×10^6	2.1×10^7	9	
^{139}Sm	2.57 min	2.8×10^5	8.4×10^6		
^{143}Sm	66 s	4.4×10^5	2.3×10^7		
^{139}Pm	4.15 min	3.1×10^5	2.6×10^7		
^{160}Tm	9.4 min	5.0×10^5	3.5×10^6		
^{164}Tm	5.1 min	9.6×10^4	1.6×10^7		
^{160}Yb	4.8 min	1.0×10^6	1.6×10^7	6	
^{160}Lu	40 s	2.2×10^4	1.5×10^7		
^{168}Lu	6.7 min	1.3×10^6	4.1×10^6		
^{143}Gd ^{143m}Gd	39 s 1.87 min	6.7×10^4	3.5×10^6		
^{145}Gd ^{145m}Gd	23.0 min 85.2 s	6.7×10^5	1.7×10^7	4	2

For ^{143}Gd and ^{145}Gd the total values of the yields summarizing the measured isomeric and ground states are given. The efficiency of the laser target for ^{145}Gd production is pointed out as well. The combined target-ion source unit efficiency, which is a product of the release and ionization efficiency, was obtained as the ratio of the measured yields to the yields calculated on the base of cross sections supplying by the EPAX code. That efficiency estimation was obtained only for isotopes with respectively long half-lives and which production cross sections are close to the maximum of the cross section curve (^{143}Eu, ^{145}Gd and ^{160}Yb). As one can see in Table 2, the on-line production efficiencies for pointed out long-lived isotopes are in a good agreement with the off-line measured values (Table 1).

3.3. The CTIS use for on-line laser spectroscopy experiment

The developed combined target-ion source unit has been used for a laser resonance spectroscopy investigation of neutron-deficient Gd isotopes [7]. The scheme of the CTIS used for the laser spectroscopy experiments is shown in Fig. 6.

For the comparison of two methods (LIS and LT), the ratio R of the photo-ion current to the thermal ionization background has been measured for two types of the target system: the first one was a traditional construction (target connected to the ion source) [8] and the second one was the laser target. In Table 3 the

beam intensities of ^{145m}Gd and ^{145g}Gd from both tested target systems at the equal temperature conditions are presented. During the tests the targets having an identical material thickness were used, which were irradiated in both experiments by the same proton beam intensity. Also we were trying to keep the same temperature conditions for the tested targets and the ion source. The temperature was (2500 ± 50)°C that ensured a rather fast escape of Gd radioactive atoms for which the effusion is considered to be the main delay dominating process. In spite of similar conditions of radioactive Gd production for both targets, we have obtained the ratio of ^{145m}Gd ($T_{1/2}$ =1.87 min) to ^{145g}Gd ($T_{1/2}$ = 23 min) almost 7 times higher from the laser target than from the usual target-ion source unit (see Table 3 "laser off"). The enhancement of ^{145m}Gd having a considerably shorter half-life than a long-lived ^{145g}Gd demonstrates that the integrated target-ion source is faster than the usual target-ion source unit.

Table 3

Beam intensities of ^{145m}Gd and ^{145g}Gd produced by different target-ion source units at a temperature of 2500°C

	^{145m}Gd beam intensity, s^{-1}		^{145g}Gd beam intensity, s^{-1}		Ratio ^{145m}Gd/^{145g}Gd	
Type of target-source unit used	Target with ion source	Laser target	Target with ion source	Laser target	Target with ion source	Laser target
Laser at resonance	$1.64(8)\times10^{5}$	$3.21(11)\times10^{5}$				
Laser off	$1.55(6)\times10^{5}$	$2.30(8)\times10^{5}$	$2.02(20)\times10^{6}$	$4.40(16)\times10^{5}$	$7.7(1.1)\times10^{-2}$	$5.20(37)\times10^{-1}$
R	0.06(6)	0.40(6)				

3.4. The uranium carbide CTIS for the production of neutron-rich isotopes

A schematic drawing of the CTIS for the production of nuclides with high ionization potentials is shown in Fig. 7. The electron beam was introduced into the target volume by a cathode shaped for that purpose and placed to the side of the extraction electrode. So the electron beam ionization took place inside the target container [3]. The yields of neutron-rich Ag and Sn isotopes are shown in Fig. 8. The production efficiency values obtained as a ratio of measured and calculated yields are, correspondingly, 4% and 2% for long-lived Ag and Sn. With a high value of probability it is equal to the ionization efficiency of that species, as the release times of these elements are shorter than their lifetimes.

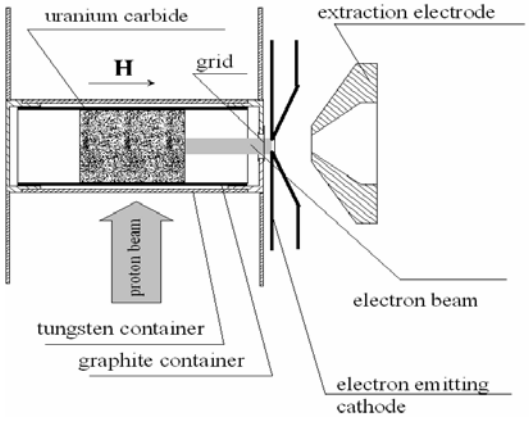

Fig. 7. Scheme of the electron beam ionizing UC target for production of neutron-rich isotopes

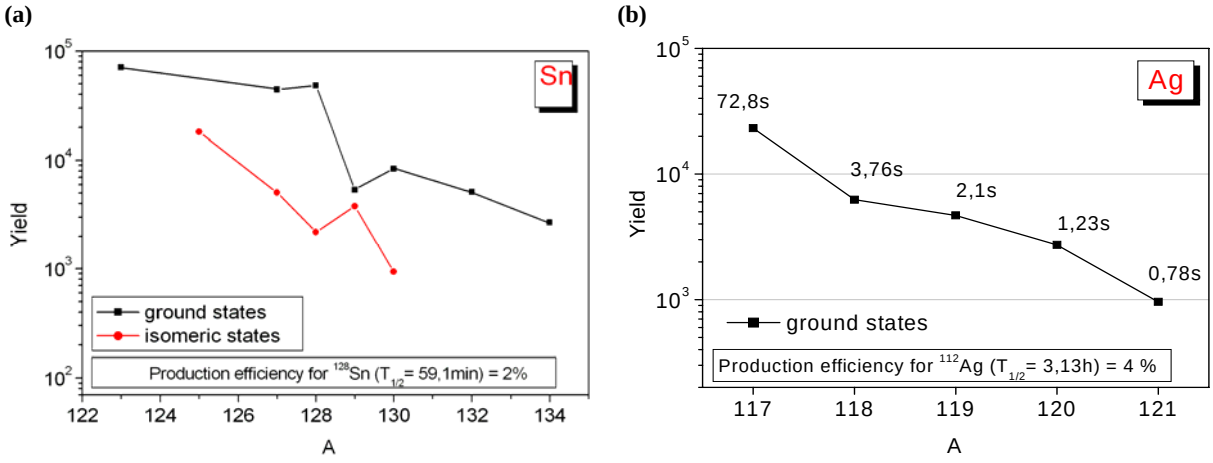

Fig. 8. Sn (a) and Ag (b) isotope yields from the electron beam IT

4. Conclusion

The yields of on-line mass-separated Cs, Rb and Fr isotopes have been studied at the IRIS. Properties of high density UC targets, in form of rod and powder, and a low density UC_x target prepared by the ISOLDE method similar to the PARRNe target are compared. According to the measured yield trends, the release efficiency of an ISOLDE like target for short-lived Cs isotopes is 1.5–2 times higher than that of a HDR (high density rod) uranium carbide target which was studied at the IRIS initially. It is rather encouraging result, as the grain size of the HDR UC target was ten times larger than the ISOLDE like target.

It should be pointed out that the on-line measured production efficiency and release properties of the ISOLDE like target specially prepared at the IRIS for that comparison tests coincide with the ISOLDE original target within the experimental errors (≤ 40%).

To compare target materials having different densities but a similar dispersivity, a new developed, high density pill (HDP) UC target with the grain size of 20 μm have been on-line investigated. According to the measured Cs yield trends, the release efficiency of the new HDP target coincides with the ISOLDE like target within the limits of the measurement errors.

The comparison of the yields of short-lived Fr isotopes from the HDR and HDP targets with the yields from the ISOLDE graphite-cloth target exhibits a rather unexpected result: the normalized yields of extremely short-lived Fr isotopes from high density targets are equal or even higher than those from the graphite-cloth target.

Off- and on-line tests of ionizing targets have demonstrated that they can be used for the on-line production of a large set of nuclides using surface and resonance laser ionization. The ionization efficiency measured off-line for surface and laser ionized different species is comparable with those published in the literature. A low ionization efficiency value for Li can be explained by a low temperature of the ionizing target. To ensure a higher Li ionization efficiency, a target temperature should be at least 2200°C or even higher. The ionization efficiency for the tested elements can be increased in our construction almost by a factor of two by decreasing the diameter of the hole for the beam from 2 to 1 mm, as the laser beam diameter is about 0.5 mm.

As it is seen in Table 2, the target can be successfully used for the production of neutron-deficient isotopes of all rare-earth elements. The ionization efficiency may be higher about 3 times, if the ionizing target is used only in a surface ionization mode when the hole for the laser beam introduction is eliminated.

References

1. V.N. Panteleev *et al*., Rev. Sci. Instr. **73**, 738 (2002).
2. V.N. Panteleev *et al*., Nucl. Phys. A **701**, 470c (2002).
3. V.N. Panteleev *et al*., Rev. Sci. Instr. **77**, 03A705(2006).
4. A. Andrighetto, A.E. Barzakh *et al*., Eur. Phys. J. A **19**, 341(2004).
5. A. Andrighetto, A.E. Barzakh *et al*., Eur. Phys. J. A **23**, 257 (2005).
6. V.N. Panteleev *et al*., Eur. Phys. J. A **26**, 147 (2005).
7. A.E. Barzakh *et al*., Phys. Rev. C **72**, 017301 (2005).
8. A.E. Barzakh *et al*., Phys. Rev. C **61,** 034304 (2000).

SYSTEM FOR DEEP PURIFICATION OF HYDROGEN IN MuCap EXPERIMENT

V.A. Ganzha, P.A. Kravtsov, V.A. Trofimov, G.N. Shapkin, A.A. Vasilyev, M.E. Vznuzdaev

1. Introduction

The MuCap experiment at PSI is a precision measurement of the rate Λ_S for the basic electroweak process of muon capture, $\mu^- + p \rightarrow n + \nu$. A measurement of 1% accuracy determines the last well-known of the nucleon charged current form factors, the induced pseudoscalar g_P, to 7%. The experiment is carried out at the πE3 muon beam of the 580 MeV proton accelerator at the Paul Scherrer Institute (PSI), Switzerland.

The capture rate is determined from a measurement of the disappearance rate $\lambda_- \approx \lambda_+ + \Lambda_S$ of negative muons in hydrogen and the world average of the free μ^+ decay rate λ_+. Muons are stopped in a time projection chamber (TPC) with sensitive volume $15 \times 12 \times 30$ cm^3 filled with ultrapure hydrogen at 10 bar. Electrons ionized by muons or other projectiles drift vertically in a homogeneous electrical field to the bottom of the TPC, where they are amplified with a multiwire proportional chamber (MWPC) and read out in two dimensions.

The experiment imposes strict and critical requirements on the hydrogen gas system supporting the active target – TPC detector. As the hydrogen gas density of the experiment of ten times higher than at standard temperature and pressure, the rates for muon transfer from μp to typical chemical impurities (N_2, H_2O, O_2) are 3 orders of magnitudes larger than the muon decay rate. Once a muon has been transferred to a μZ atom, nuclear muon capture proceeds more than 100 times faster than on a μp atom. Thus, gas impurities distort the observed lifetime spectrum, and transfer must be suppressed by keeping the gas contaminations below a level of typically 10 ppb. Isotopic purity is required as well, since muon transfers to deuterium lead to a difficult diffusion problem. A dedicated isotope separation device [1] was constructed to produce protium with a deuterium contamination of less than 70 ppb; this work will be published separately.

As the gas amplification in the MWPC of the TPC sensitively depends on the hydrogen pressure, the pressure inside the TPC must be stabilized on the level of 10 bar with 0.1% accuracy. This is required to keep the MWPC gas gain constant within 1%. There is also concern that large flow variation in the TPC might induce dust accumulation and breakdown of the chamber high voltage. Thus the flow has to be stabilized as well. Finally, the whole detection system operated with high voltage in a pure hydrogen environment, thus reliability and hydrogen safety were of utmost importance.

The "Circulating Hydrogen Ultrahigh Purification System" (CHUPS) was designed and built to provide continuous protium purification and achieved all design criteria over several experimental runs with typically 2 months of continuous operation per year.

2. Circulating system (CHUPS) design

2.1. CHUPS operation scheme

During the experiment the TPC can directly monitor the capture reactions on impurities, the yield roughly proportional to the impurity concentration. This technique was used in 2003 before CHUPS was installed, showing the yield increasing during several days after filling the TPC. The chamber was filled through the palladium filter and exposed to the muon beam. The experiment revealed accumulation rate of some tens ppb per day which is unacceptable for the experimental requirements. This is the main reason for development of CHUPS designed for continuous gas cleaning and circulation through the operating TPC.

Initially a circulation system consisting of a mechanical pump and a Pd filter was considered. Pumps with high vacuum rating operating at 10 bar pressure are not commercially available and Pd filters supporting the required flux of 3 slpm (standard litres per minute) are expensive. Instead the alternative CHUPS scheme was realized, which is based on an adsorption cryopump to maintain the hydrogen flow and a cryogenic adsorption filter for removing the impurities. The adsorption cryopump has essential advantages, such as intrinsic high purity and reliability due to the absence of moving parts. The circulating system was designed, mounted and tested at PNPI in Gatchina, Russia, and installed at PSI during the preparation period

of the MuCap experiment in 2004 [2]. It was upgraded in 2005 on the basis of the operating experience. A simplified diagram of the system is shown in Fig. 1. CHUPS consists of two main units which are mounted separately on a common frame: compressor and purifier.

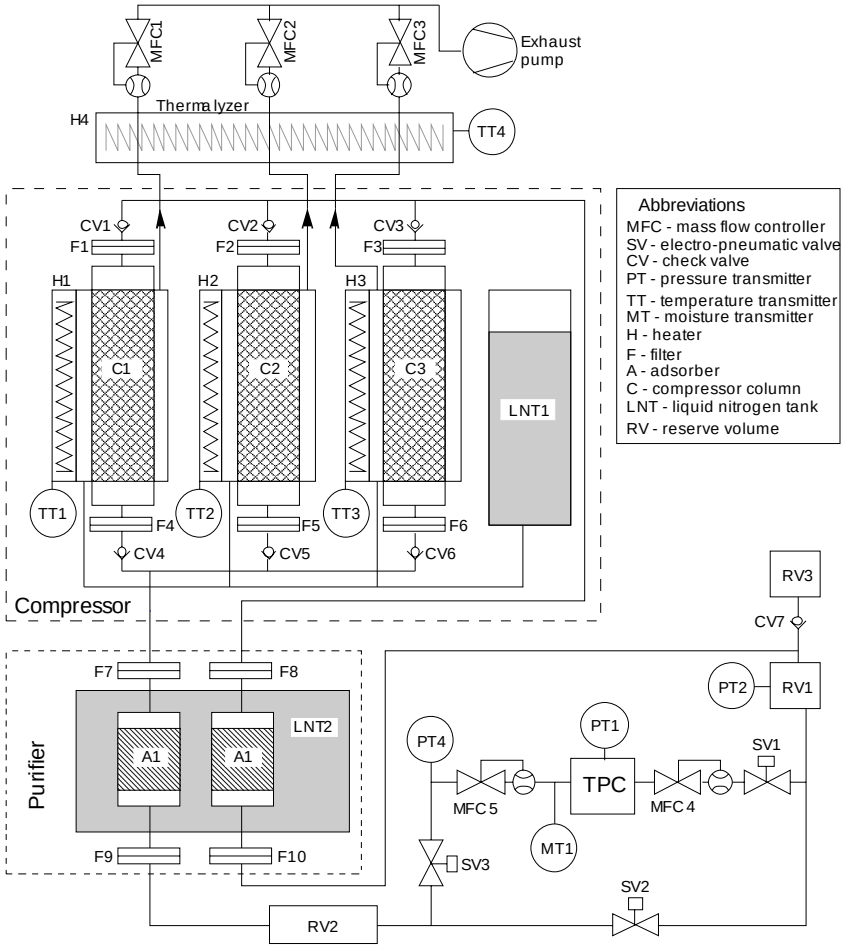

Fig. 1. Simplified CHUPS diagram

2.2. Compressor

The compressor is a triplex adsorption cryopump. It has three identical cartridges (columns) filled with activated carbon [1] and connected in parallel. The cartridges are made from thick-walled stainless steel tube and designed to keep high pressure. The volume of each column is about 1 liter and contains with respect to packed density of the carbon up to 0.6 kg of the adsorbent. Each column (C1, C2, C3 in Fig. 1) has a heat exchanger made of copper tube. It is coiled around the column and soldered to its outer surface by silver hard alloy. The heat exchanger is used to cool down the compressor column using liquid nitrogen flowing from the 40-litre supply vessel (LNT1). Liquid nitrogen flow is provided by an exhaust pump connected to the heat exchangers manifold. After cooling the columns nitrogen flows through the thermalizer (H4), which heats the gas up to the room temperature. Mass-flow controllers [2] MFC1, MFC2, MFC3 control the flow rate of the gaseous nitrogen and consequently regulate the liquid nitrogen flow rate and the cooling rate of the column. An electric heater is coiled around the column between the heat exchanger turns to provide the column heating. Each column has two check valves with the actuation pressure of 50 mbar that are installed in the inlet and outlet pipelines (CV1−CV6). Inlet and outlet lines of the columns are combined to the inlet and the outlet manifolds, respectively.

[1] Norit Nederland B.V. Nijverheidsweg Noord 72, 3800 AC AMERSFOORT, The Netherlands.
[2] Aalborg (http://www.aalborg.com/) stainless steel GFC series mass-flow controllers.

At the cooling stage the adsorbent inside the column adsorbs hydrogen, and the internal pressure drops below the pressure in the inlet line of the compressor. Consequently, the inlet check valve opens and passes hydrogen into the column. During the heating stage the adsorbent desorbs hydrogen, and the column internal pressure rises above the outlet line pressure. The outlet check valve opens and passes hydrogen into the outlet line. Thus, the combination of the check valves provides a pulsating flux of hydrogen in one direction. Cooling and heating rates are regulated by the balance of liquid nitrogen flow (controlled by MFC1, MFC2, MFC3) and heating power (managed by pulse-width modulation of the power supplies).

The temperature phases of the columns are shifted with respect to each other. Upper and lower temperatures and cycle frequency are regulated in accordance with the required average flow rate. A single compressor column pumps approximately 32 standard liters of hydrogen in one cycle employing a temperature range of 80–150 K. The maximum hydrogen flow of 3 slpm through the compressor is defined by the maximum cooling rate and the thermalization time of the activated carbon.

2.3. Purifier

The purifier contains two cartridges filled with NaX-type zeolite [3] (indicated as adsorbers A1 and A2 in Fig. 1). The adsorbers are immersed into liquid nitrogen vessel (LNT2) and permanently kept under temperature of 77 K during the whole experimental run. Low temperature is essential to increase the adsorption ability of zeolite for high-boiling contaminants (oxygen, nitrogen) against the main gas (hydrogen). Two adsorbers contain about 40 g of the sorbent in total, enough to accumulate up to 1 g of adsorbed water. The total amount of water supplied by the flow of 3 slpm during the two-month experimental run was about 2×10^{-2} g (allowing for 100 ppb constant humidity), which is 2% of the adsorber capacity. The adsorption capacity for other contaminants is comparable. Thus, the adsorbers guarantee full impurity removal in the hydrogen flow during the long term experiment. The adsorbent has to be exchanged or can be regenerated by heating up to 400°C and pumping before each experimental run.

The liquid nitrogen vessel is contained in the vacuum case and protected from external thermal radiation by a copper shield mounted on the secondary liquid nitrogen vessel which is also used to cool down the incoming hydrogen. This technique decreases liquid nitrogen consumption and prevents heating the zeolite adsorbers. The two adsorbers of the purifier (A1 and A2) are mounted on the hydrogen lines upstream and downstream of the TPC, respectively, providing two stage purification of the gas. The inlet zeolite adsorber takes out most of the impurities, which helps to avoid any decrease of the compressor capacity due to the accumulation of impurities in the activated carbon.

The system is equipped with mechanical 2 μm filters installed before and after the compressor and in the detector pipelines that prevent carbon or zeolite dust penetration to the clean part of the system. The final purification is provided by a special gas purifier [4] of limited capacity installed at the TPC inlet.

2.4. Control system

A special stand-alone microcontroller block provides all necessary regulation algorithms. The control block is connected to a PC *via* RS-232 or RS-485 serial interface. Due to implementation of all control algorithms in the independent control block, the system remains operational in the case of computer failure. Computer software is used for adjusting the parameters of the regulation algorithms, collecting and visualizing the process variables and keeping them in the database. All system events (including software messages and alarms) are also saved in the database. Special software was developed to access the parameters history and event log in the database.

The control block measures and controls all system devices like pressure sensors, valves, mass-flow controllers, *etc.* It provides the following regulation procedures:

- temperature stabilization of the three compressor columns and the thermalizer by regulating the heating and cooling provided by the heaters and the nitrogen mass-flow controllers, respectively;

[3] CECA company, http://www.adsorbents.com/sites/ceca/en/home.page.
[4] SAES Pure Gas - MicroTorr Ambient Temperature Gas Purifiers. http://www.puregastechnologies.com/microt.htm.

- cyclic operation of the compressor columns with phase shift;
- TPC internal pressure stabilization using mass-flow controllers;
- temperature stabilization of the humidity sensor.

Alarm and interlock functions are also implemented in the control block firmware (see Table). It protects the detector from underpressure and overpressure and controls differential pressure between the TPC and reserve volume RV1 to avoid hydrogen flux variations. Also, the software tracks liquid nitrogen level in the compressor tank (LNT1) and compressed air pressure that is used for the electro-pneumatic valves (SV1–SV3) actuation. All alarm events are attended with light and sound signal.

Table

Alarm events and interlock actions

Alarm description	**Condition**	**Action**
TPC pressure high	PT1>PT1max	Cut-off TPC and open bypass
TPC pressure low	PT1<PT1min	Cut-off TPC and open bypass
Differential pressure high	(PT2-PT1)>DPmax	Cut-off TPC and open bypass
Differential pressure low	(PT2-PT1)<DPmin	Cut-off TPC and open bypass
Compressed air pressure low	PT3<PT3min	Alarm signaling
Liquid nitrogen level low in LNT1	N2Level<N2Levelmin	Alarm signaling

2,5, TPC pressure and flow control

The three columns of the compressor induce the hydrogen flow to exchange the gas in the TPC. This flow is pulsating because of the periodical mode of the column operation. The pressure inside the TPC must be stabilized with 0.1% accuracy. In order to smooth the pressure variations caused by compressor, the CHUPS system is equipped with two reserve volumes of 15 liters content each (RV1 and RV2), pressure sensors (PT1, PT2, PT4) and mass-flow controllers (MFC4 and MFC5).

The reserve volumes are installed in the inlet and outlet lines of the TPC. They are used as buffering volumes. The RV1 also provides a hydrogen reserve to support the pressure stabilization algorithm. Each volume is equipped with a pressure sensor (PT2 and PT4, same model as PT1). Two mass-flow controllers with a maximal flow of 20 slpm are mounted at the inlet (MFC4) and outlet (MFC5) lines of the TPC.

The internal pressure of the detector (measured by PT1) is stabilized using PID (Proportional-Integral-Derivative) regulation. The mass-flow controller at the detector outlet (MFC5) is set to a constant flow rate. The TPC inlet mass-flow controller (MFC4) is operated by PID algorithm in the control software. The MFC5 set point defines the average flow rate through the TPC vessel. The pressure distribution histogram (Fig. 2) for the long term operation during 50 days shows excellent pressure stability on the level of 0.024% at a mean hydrogen flow of 3 slpm. The histogram bars correspond to the ADC discretization in the control system (1.2 mbar). Thus the pressure is kept within ±2 least significant bits of the ADC. The second reserve

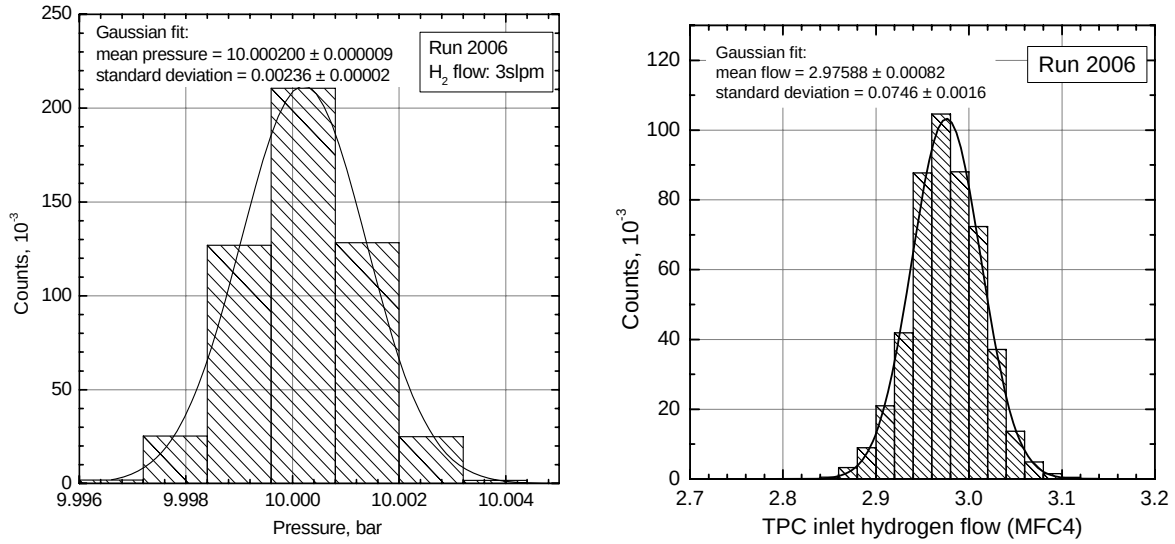

Fig. 2. TPC pressure and inlet flow distribution histograms. The gaussian fits gives a full width of 2.4 mbar and 0.075 slpm that correspond to 0.024% and 2.5% stability, respectively

volume (RV2) and the mass flow controller (MFC5) at the compressor inlet were installed to prevent pressure drops caused by the fast opening of the check valve. This results in a flow stability of 2.5% at the mean flow level of 3 slpm during 50 days of CHUPS operation (Fig. 2).

3. Monitoring impurities

The initial purity of the evacuated TPC system was provided by continuous pumping and baking of the TPC vessel. The residual gas contents were controlled by a quadrupole mass-spectrometer in the mass range from 2 to 100 atomic mass units (a.m.u.). During the protium runs atmospheric gases (oxygen and nitrogen) were analyzed by off-line gas sample chromatography, and the moisture of the gas was directly monitored with an on-line humidity sensor. The total amount of impurities was continuously monitored by direct measurements of the yield of muon capture on impurities as observed in the TPC.

3.1. Chromatographic analysis of nitrogen and oxygen

The oxygen and nitrogen content is measured by gas chromatography with a thermal conductivity sensor. After being filtered and purified in a cryogenic adsorption purifier, helium carrier gas is distributed in two directions with equally adjusted flow rates. The first flow passes through the reference chromatographic column. The second flow can be either routed to the working chromatographic column directly or through the accumulating column using the volume batcher which injects the fixed volume into specified direction. Both chromatographic columns are filled with a specially treated adsorbent (zeolite). The adsorbent in the working column separates the admixtures, while the one in the reference column provides a hydraulic resistance equal to the working column.

Preparatory enrichment is required for the very low concentrations of impurities in the hydrogen gas samples. Hydrogen from the sample bottle is directed to the accumulating column by the batcher. This column is filled with zeolite and immersed into a liquid nitrogen vessel at 77 K temperature. The amount of gas passed through the accumulating column is measured by a rotary drum gas meter. Impurities from the gas stream are adsorbed by the zeolite and remain in the accumulating column. After the desired amount of sample gas has passed through the adsorber, the accumulating column is removed from the cryogenic vessel and heated. Then the batcher directs the helium carrier gas flow through the accumulating column which washes the impurities out of the adsorbent.

In the next step, the carrier gas enriched by contaminants flows through the working column, where contaminants are separated on the adsorbent. Both reference and working flows pass through the detector in parallel, that measures their differential heat conductivity. The differential output signal is proportional to the admixture concentration. Signal peaks are registered by a PC and processed by special software. The enrichment coefficient (the sample volume passed through the accumulating column) and parameters of the measuring scheme are adjusted with respect to the admixture concentration. The final calculation of the concentration is based on a calibration measurement. A serial dilution method was used to obtain the set of calibrating samples with decreasing concentration of nitrogen and oxygen. With this method a sample of the air was serially attenuated by the hydrogen. The total calibration error, including non-linearity, is 10%. The traces of the main air components were monitored by gas samples of 8−10 normal liters from the TPC using the chromatographic method. A sensitivity of 5 ±1 ppb for oxygen and 7 ±1 ppb for nitrogen was obtained.

3.2. Humidity analysis

During the MuCap experiment 2004 we observed a capture yield corresponding to about 60 ppb impurities, significantly higher than the oxygen and nitrogen concentration derived from the gas chromatography

In 2005 an online humidity sensor [5] was installed to investigate whether the additional observed yield can

[5] Pura PUR-TX-120 Gas Dew-point Transmitter.MichellInstruments. http://www.michell.co.uk/cat/view/pura.html

be explained by residual water vapor in the hydrogen gas. The sensor has sensitivity of 0.02 ppb with error of +30–50% in the 2–100 ppb range. It was mounted in a temperature-stabilized box in order to reduce any influence of the ambient temperature to the sensor reading. Sensor and inlet pipeline were kept at 21°C with 0.2°C stability. As shown in Fig. 1, the humidity sensor (MT1) was installed in the gas circuit such that it could measure either the humidity in the outlet TPC flow or in the isolated CHUPS system (while hydrogen is circulating through the chamber bypass). Continuous bypass circulation gave 3 ppb humidity. During the production run the humidity sensor clearly demonstrated that humidity was the main additional impurity. To calibrate the effect of H_2O impurities on the experiment, a water permeation tube [6] was used for generation of the known water concentration in the hydrogen flow. The tube was placed in the temperature stabilized vessel. Stable hydrogen flow was passed through the volume with the tube.

3.3. Impurity capture rates

The specifics of the MuCap experiment allow unique in-situ measurements of impurity concentrations during the experimental runs. While the vast majority of negative muons remain in muonic hydrogen atomic (μp) and molecular ($p\mu p$) states during their lifetime, a small fraction can be captured on impurities in the following steps: $\mu p + N_Z \rightarrow \mu N_Z + p$; $\mu N_Z \rightarrow N_{Z-1} + \nu$. Here N_Z is a nucleus of an impurity atom, like N or O. The first transfer reaction proceeds with a rate proportional to the impurity concentration c_Z. The second capture reaction occurs with a probability $\Lambda_Z/(\Lambda_Z + \lambda_+)$, which is the result of the competing processes of capture with rate Λ_Z and free muon decay with rate λ_+. The charged recoil nuclei N_{Z-1} are detected in the TPC. The observed yield of capture recoils per muon is $Y_Z = c_Z k_Z$, where k_Z are coefficients which depend on Λ_Z and the detection efficiency for recoil N_{Z-1}. They are determined in dedicated calibration runs where hydrogen is doped with a single impurity N_Z of well measured concentration c_Z, typically 100–1000 times higher than in the clean run conditions. Typical values are $k_N = 70$ and $k_O = 400$ for both Y_Z and c_Z in ppm (the detection efficiencies slightly differ from run to run). In summary, the capture yield measurement allows a continuous and precise measurement of the overall observed capture yield from impurities, but it does not distinguish between their elemental composition.

4. Operating experience

4.1. Clean fills for production data

Before the 2004 experiment the TPC was baked for several weeks. The performance of the gas system over the whole run period is documented in Fig. 3. The chromatographic analysis allows monitoring the change of oxygen and nitrogen concentrations during the MuCap experimental run. Fig. 3 shows the behavior of nitrogen concentration for the MuCap experimental run after starting the CHUPS. The final chromatographic measurements resulted in nitrogen concentrations less than the method sensitivity (7 ppb). Oxygen traces dropped below the method sensitivity of 5 ppb within two days after starting the circulation.

The most reliable drying experience was obtained during the spring 2006 experimental run. Before the run, the TPC had been exposed to continuous (about 2 months) vacuum pumping with a simultaneous baking at ~120°C. This procedure led to an initial humidity level at the moment of CHUPS connection of 60 ppb (Fig. 4, left). During 400 hours of continuous cleaning with a mean hydrogen flux rate of 3 l/min the humidity exponentially decreased to ~18 ppb and remained at this level till the end of the main μ^- data run, providing a stable operation over more than 1000 hours. The minor fluctuations of the humidity are explained by temperature fluctuations in the experimental hall. The change of hall temperature affects the adsorption-desorption equilibrium in the chamber and, consequently, its outgassing rate. Then CHUPS was disconnected from the TPC and run through bypass line. The humidity decreased exponentially and reached the 10 ppb level in 20 hours (Fig. 4, right). The final CHUPS stand-alone humidity result is 3 ppb.

[6] Permeation tube providing 500 ppb ± 10% at 0.5 slpm flow. Valco Instruments Company Inc. P.O. Box 55603, Houston, TX 77255, USA.

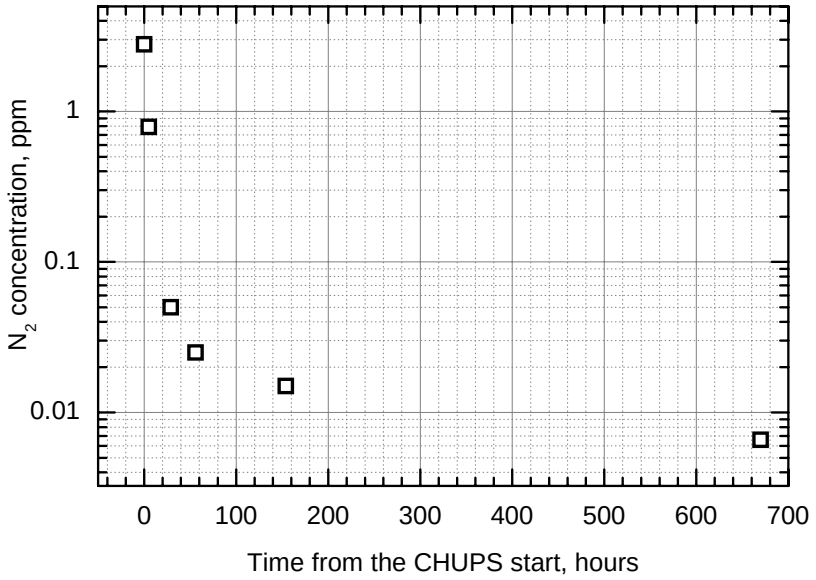

Fig. 3. Nitrogen concentration change during MuCap run 2004. Average hydrogen flow is 1.6 l/min

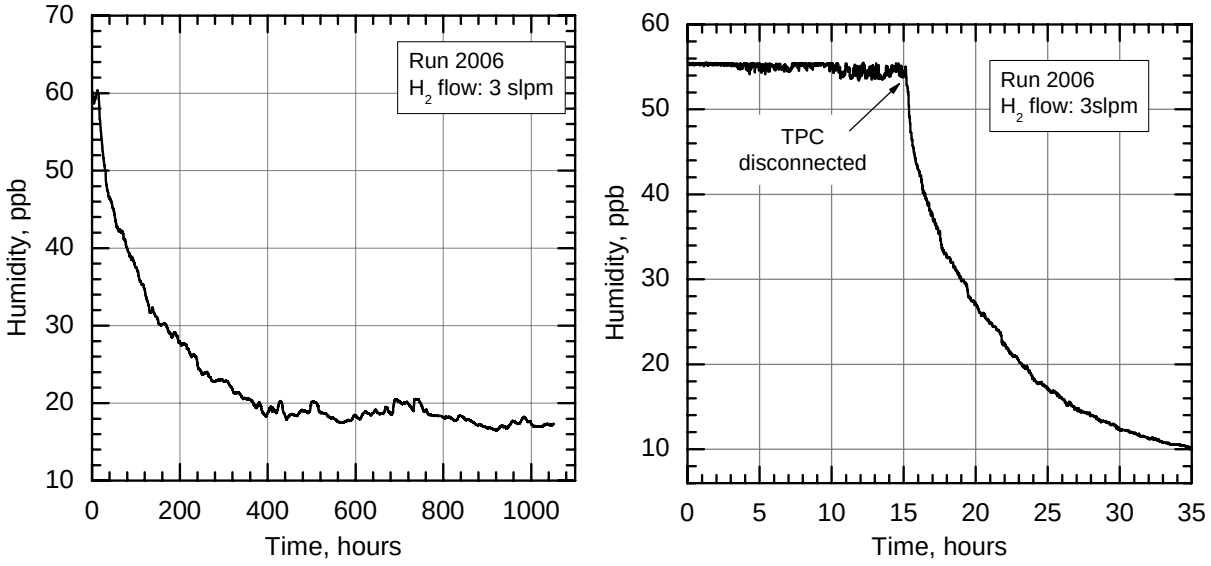

Fig. 4. Humidity decrease in the TPC after CHUPS connection (left) and after bypassing the TPC (right)

4.2. Impurity doped fills for calibration data

The cleaning power of CHUPS was greatly confirmed during systematic calibration studies of the TPC detector which were carried out during the last weeks of the MuCap experimental run in spring 2006. Several experiments were carried out for the TPC calibration and the determination of the major impurities. The high cleaning power of the CHUPS system makes it possible to return the detector to the normal clean operation in a short time.

The first experiment was a "water doped run". During this test the humidity inside the TPC was increased up to 2000 ppb approximately by a specially prepared humidity generator. Then CHUPS was connected and the gas was cleaned down to 400 ppb in one day (Fig. 5). The slower cleaning speed can be explained by wetting of the inner surfaces of the chamber.

The efficiency of CHUPS cleaning a large contamination of nitrogen in the detector hydrogen was tested by adding a "high" 22 ± 1 ppm nitrogen admixture from a known amount of nitrogen previously diluted

in a vessel with high purity protium. This "nitrogen doped" condition was intended as a detection efficiency calibration of nitrogen impurity capture events in the TPC. After measuring with the large nitrogen contamination (flat region) the CHUPS circulation through the TPC vessel was re-established and the nitrogen was removed. The cleaning progress observed on-line *via* capture events in the TPC is shown in Fig. 6. The cleaning started with a yield of more than 1000 ppb and proceeded until leveling off around ~30 ppb, a value established before the doping. The purification process took about 17 hours.

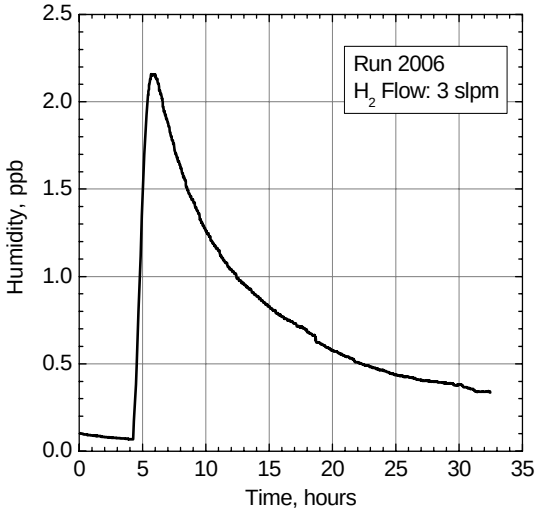

Fig. 5. Drying of TPC after the water doped run

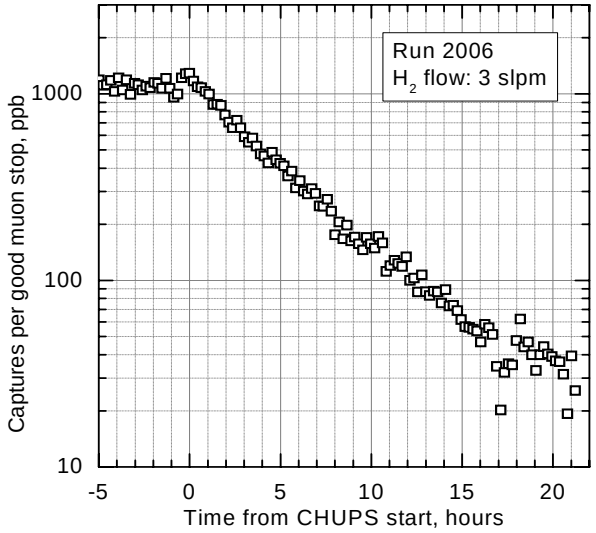

Fig. 6. Impurity captures per good muon stop during the nitrogen cleaning

4. Results

The CHUPS system was installed in the MuCap experiment at PSI and first connected to the TPC detector in 2004. The system proved to be very reliable and flexible during three experimental runs in 2004–2006.

The experience obtained during development and use of the CHUPS justifies the initial design decisions. The main result was a stable clean working gas of the TPC during the experimental runs. A smooth hydrogen flow of 3 l/min was kept during the whole TPC operation time (more than 1000 hours in one experimental run). The best purity reached was 18 ppb for moisture content and 8–10 ppb for nitrogen concentration. This result is sufficient to reach the main goal of the MuCap experiment and allows precise corrections of the proton capture rate for these impurities. In addition to regular cleaning, the CHUPS provided fast cleaning of the working gas after calibrations with contaminants doping. This feature was very useful for the nitrogen and water calibration experiments intended for systematic studies of the TPC detector. Also, variations of the CHUPS flow and correspondingly the equilibrium humidity in the chamber gave important additional calibration points for the systematic investigations.

With regards to the stable pressure requirement the CHUPS also yielded a good result. The pressure inside the TPC was kept at the appropriate level of 10 bar with 0.024% stability during all the operation modes. Pulsations of the hydrogen flow through the TPC chamber were also minimized to the level of 2.5% at the mean flow of 3 l/min.

References

1. I. Alekseev *et al.*, Preprint PNPI-2702, Gatchina, 2006. 26 p.
2. B. Bezymyannykh *et al*., Preprint PNPI-2611, Gatchina, 2004. 17 p.

HYDROGEN DISTILLATION AT THE DEUTERIUM REMOVAL UNIT OF MuCap EXPERIMENT

I.A. Alekseev, E.A. Arkhipov, S.D. Bondarenko, O.A. Fedorchenko, V.A. Ganzha, P.A. Kravtsov, V.A. Trofimov, A.A. Vasilyev, T.V. Vasyanina, M.E. Vznuzdaev

1. Introduction

The MuCap (Muon Capture on the Proton) experiment has been carried out during 1998–2006 at the Paul Sherrer Institute (PSI), Switzerland. The goal of this experiment is to measure the rate of the basic electroweak process of muon capture with hitherto unachievable high precision (1%). This measurement will provide an estimation of the nucleon charged form factor g_P with all-time high accuracy ~ 7%.

The method needs a very precise measurement of the muon lifetime in the $\mu^- p$ system in comparison with the lifetime of the free μ^+. To achieve this precision, ultra pure and deuterium depleted hydrogen gas (so-called protium) must be used. It is necessary to avoid transfers of μ^- to impurities or deuterium nuclei. These transfers lead to spoiled time spectra. A new experimental technique based on high pressure time projection chamber (TPC) filled with protium was used for the measurements. The experiment imposes strict and critical requirements on the hydrogen gas system supporting the detector. Desirable overall part of contaminants is about 10^{-8} for chemical impurities and 1×10^{-7} for deuterium. Circulating Hydrogen Ultrahigh Purification System (CHUPS) was built to provide the permanent purification of protium from the chemical contaminants during an entire statistics run (up to 2 months of continuous operation) [1]. This system was recently equipped with the Deuterium Removal Unit (DRU) – device for manufacturing of ultra pure protium from hydrogen [2]. A principle of hydrogen cryogenic distillation was used as a basis for the unit design.

The rectification method uses the difference in saturation vapor pressure of separating species above the surface of the mixture. This facility can be either a set of perforated plates or particular packing. The packing is more suitable for a column with a relatively small inner diameter. On the top of the column a condenser is placed which condenses vapor and returns it into the column in the form of liquid (reflux). The vapor from the top of the column can be partially taken away from the column as a product of the process. The reflux drains down along the column moistening the packing. An amount of the liquid suspended on the packing is a column holdup. Lower end of the column is equipped with reboiler. A separated mixture boils in the reboiler forming the vapor. The vapor rises upward along the column and interacts with the counterflow of draining reflux: the liquid is saturated by the high-boiling component, and the gas – by the low-boiling one.

In our case of hydrogen-deuterium separation a separating mixture is the mixture of regular hydrogen (H_2) and "deuterohydrogen" (HD). D_2 molecules are extremely rare and should not be considered. Besides, there is a division of the H_2 molecules into two groups, one of which has its protons aligned in the same direction (referred to as orthohydrogen) and the other in opposite directions (parahydrogen). Ordinarily, transition between ortho and para forms are relatively rare, so H_2 can be considered as a mixture of two distinct components. The ratio between the ortho and para forms is about 3:1 at standard temperature and pressure, but the para form dominates at low temperatures.

Separation factor α defines an elementary separation effect achieved at one contact of liquid and vapor hydrogen. Ideal separation factor is a ratio of saturation vapor pressures above pure components, it depends on temperature: the higher temperature the lower separation factor. But the separation factor for deuterium-protium is much larger than for ortho-para hydrogen at the same temperature. Throughout the contacting tower, liquid and vapor are brought into repeated contacts that multiply elementary separation effect. Thus the flowing down liquid hydrogen becomes steadily enriched in deuterium and orthohydrogen while the rising vapor becomes steadily depleted. According to the concept of Equilibrium Theoretical Plate, Height Equivalent to a Theoretical Plate (HETP) is the main performance characteristic of a separation column. HETP is the height of a part of a column left by liquid and gas flows which are in equilibrium to each other, (*i.e.*, for example, deuterium concentration in the liquid is α times higher than in the gas). The lower HETP value the higher column's separation power.

The column was designed to be operated so as to separate the initial mixture injected into the column through a feed port withdrawing pure H_2 (with deuterium content at least 30 times lower than in feeding gas) as distillate product and discarding the HD component in the reboiler stream. For the safety reasons and to select the most suitable operating mode, a number of studies and verifications were carried out. They include checks of the mechanical design and integrity and investigations of the pressure drop, the liquid holdup and column performance at different modes. Also, these investigations are very important to evaluate the accuracy of the measurements. The results of these studies are reported here.

Inefficiency of low deuterium content analysis in protium and the fact that possible residual deuterium content of the depleted product can be lower than the detection limit complicate the verification of separating power. It has made us find another approach. The use of gas chromatography method for ortho-para hydrogen analysis was found as a relatively fast and simple way of column performance evaluation. Also, low deuterium probes were measured on the small accelerator built specially for isotope analyses with special ion source giving extremely low backgrounds of hydrogen ions.

2. The mechanical design of the deuterium removal unit

The simplified layout of the DRU is presented in Fig. 1. Separation column of 2.2 cm inner diameter and 155 cm overall packing height is the main part of the unit. It consists of two sections connected with ISO CF40 flange coupling and is cased in a vacuum jacket. The 2.5 m vacuum jacket fixed on tripod is a basis for the setup. All working parts of the device are placed inside the jacket and its upper and lower attachments (so-called adaptors). The jacket and the adaptors comprise a common vacuum volume.

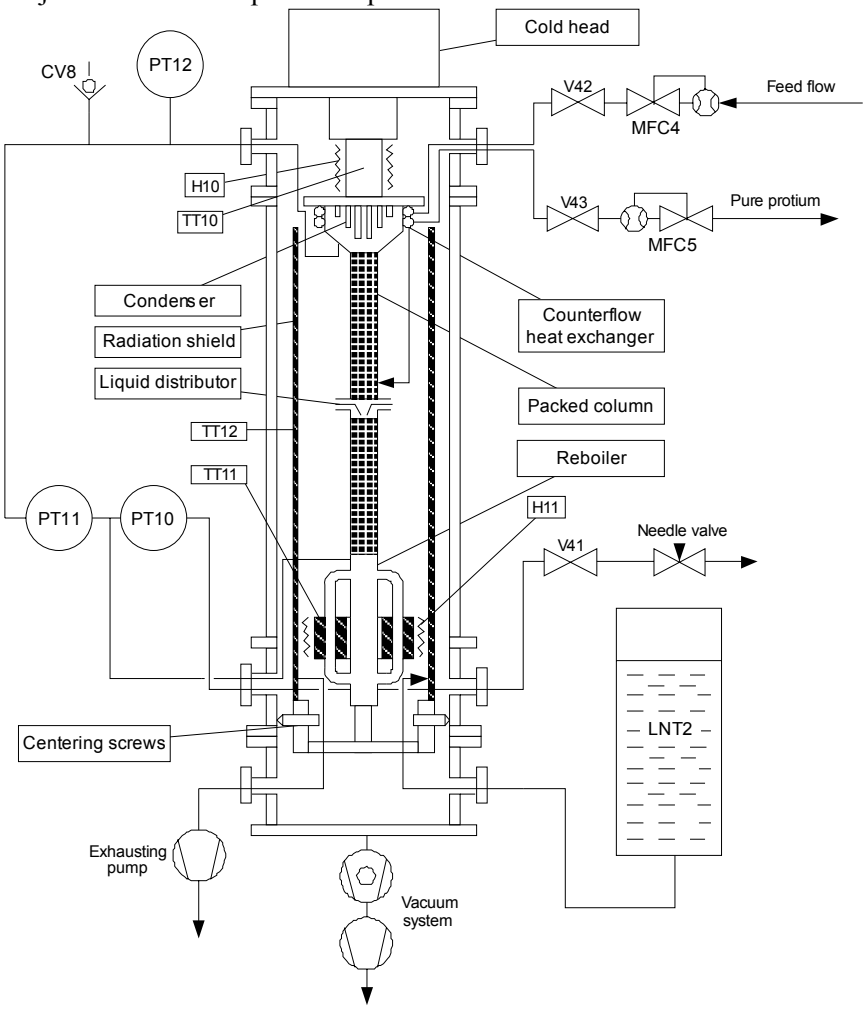

Fig. 1. DRU simplified diagram

The column has a condenser and a reboiler connected with its upper and lower parts. A COOLPOWER 140T (Leybold vacuum GmbH) cryogenerator was used for the cold operations, with the maximal cooling power of 20 W at 20 K.

A conical liquid distributor is fixed between the upper and lower sections of the column. Both sections of the column are filled with random packing. The liquid feed stream (see comments below) is introduced into the bottom of the upper section of the column. The distributor is intended to collect the liquid trickling down from the upper section and guide it to the center of the lower section. It is essential to prevent the effect of "adhesion" of the liquid to the column's wall.

The control system provides the algorithms necessary for column's operation in all modes. It operates two mass-flow controllers (MFC4 and MFC5) and two heaters (H10 and H11) and measures temperature and pressure sensors.

2.1. Condenser

The condenser is a closed conical bimetallic volume (Fig. 2, left). Its flat upper part is made of 10 mm copper plate. Inner part of this plate is processed in a form of a row of lamellas to develop the heat transfer surface area. Vertical orientation of the lamellas provides easy sliding of hydrogen condensed drops downward. The conical part has a flange for connecting to the column and welded to the copper plate by electron-beam. The condenser has two connections (tubes with 1 mm internal diameter) for conducting product hydrogen and its pressure to an upper point of the differential manometer PT11.

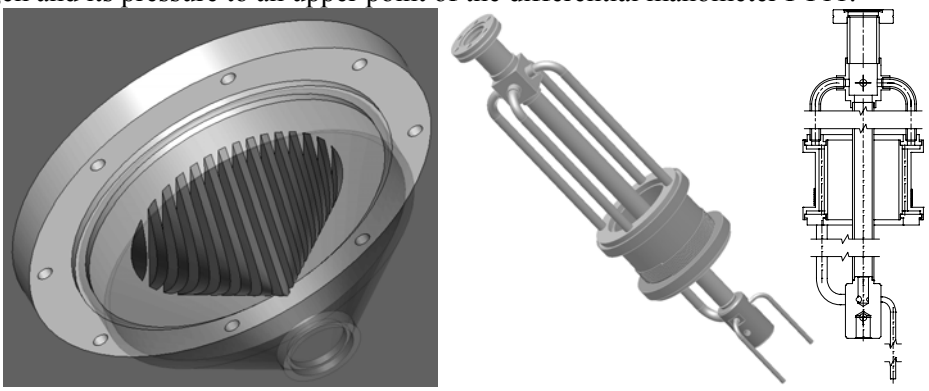

Fig. 2. The condenser (left) and the reboiler (right)

The cold head tightly contacts with outer surface of the copper plate through an indium foil. The cooled part of the condenser is mounted in the upper adaptor and that way in the common vacuum insulation of the column. A counterflow heat exchanger is mounted around the condenser and fixed on its upper flange. It cools down the feeding flux flow (inlet flow) by the deuterium depleted product flux (outlet flow).

2.2. Reboiler

The reboiler (Fig. 2, right) is essential to supply evaporation of the separating mixture. It has rather complicated arrangement to provide steady controllable boiling. This unit consists of central pipe, copper muff, upper and lower collectors and several connecting tubes. The central pipe keeps the most of liquid hydrogen collected in the bottom of the column. Both of collectors are welded to the pipe. The lower collector is also connected to the boiler by the short connecting tube. The massive copper muff has a large central hole. Several longitudinal apertures are drilled in the muff around the big hole. Their outlets are opened into common upper and lower grooves which are closed by stainless steel covers. The covers are welded to the boiler's body. Bimetallic structure allows the boiler to have very good heat conductivity owing to the copper body and therewith solid connection with other steel parts through the steel covers. The boiler is equipped with electric heater coiled around its body and PT100 thermometer to control its temperature. Liquid hydrogen boils in the longitude apertures and its vapor moves upward through four long connecting tubes. The short connecting tube provides a circulation between the lower collector and the boiler.

The advantage of the considered assembling is the separation of main amount of liquid hydrogen from the boiling section. Because of this separation, we obtain a steady level of liquid hydrogen inside the central pipe, which is measured by a differential manometer PT10. The low pressure point of this manometer is

connected to lower part of the column and the high pressure point – directly to the lower collector. ISO CF16 and CF40 connections are used for coupling of column parts. This type of connection is characterized by excellent vacuum tightness and good temperature cycling reliability.

2.3 Packing

The column is filled with specially designed spiral prismatic random packing made from 0.2 mm stainless steel wire. The packing is intended to provide a maximal surface of phases contact. At the size of the prismatic springs of 2 mm × 2 mm and total volume of packing in the column 560 ml it gives surface of 1.95 m^2. The choice of stainless steel as a material is caused by purity conditions of hydrogen. The packing surface was pickled by nitric acid to develop its roughness and improve wettability by liquid hydrogen.

It was the first test of the packing in a cryogenic distillation column. This type of packing (but bigger size – 3 mm × 3 mm) was earlier tested in PNPI's water distillation columns of 80 mm inner diameter and showed good separation characteristic (HETP = 2.5–3 cm) [3]. The similar packing made from stainless steel tested in cryogenic distillation column of small diameter gives HETP value about 5–6 cm. That is why the value of HETP equal to 5 cm was put in the design according to conservative approach.

3. Experiments and results

In April–May 2006 the DRU was tested during a few long (up to 7 days) periods of operation. The total amount of pure protium produced by the column in this run was 1300 litres. Almost all tests of columns performance were carried out at so-called "total reflux mode", with zero feed flow and correspondingly withdrawal flows from the column top and bottom.

3.1. Analysis

The analysis of low deuterium content in hydrogen is not prompt and besides the residual deuterium content of the depleted product can be lower than the detection limit. Nevertheless, a method for fast estimation of column performance was strongly needed. A chromatographic analysis of ortho- and para-isomers of hydrogen was proposed as a method of indirect estimation of the column separation power.

For the analysis the same chromatographic device was used as for analysis of nitrogen traces. However there are some changes introduced into the device for this specific method of analysis. The first distinction was the use of Al_2O_3-filled chromatographic column immersed into liquid nitrogen. The liquid nitrogen temperature is essential to provide the separation of the isomers that have temperate difference in adsorption affinity. The other essential difference is the direct injection of the sample into the carrier gas without the preliminary accumulation of impurities. The accumulation is unnecessary because of relatively high concentration of the separated components. The third serious property of this method was the use of neon as the carrier gas. It was used to provide more difference in thermal conductivity between the separated species and carrier gas in comparison with conventionally used helium.

Measurement of the concentration of ortho- and para- isomers in the top and bottom parts of the column allows to estimate its separation performance and recalculate the concentration profile for deuterium. A sample of chromatogram for samples taken from the top and bottom part of the column is shown in Fig. 3.

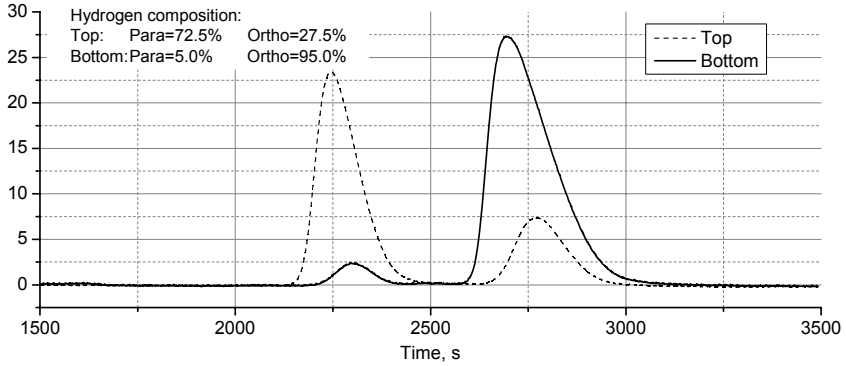

Fig. 3. Chromatogram of separated ortho- and parahydrogen (column pressure = 1.2 bar; reboiler power = 10 W; operation mode: total reflux)

Separation ratio is the ratio of relative concentration of a component of interest at the bottom to the top of the column: $SR = \frac{X_{Bottom}/(1-X_{Bottom})}{X_{Top}/(1-X_{Top})}$. If separation factors are known for the total reflux operating mode the recalculation of ortho-para hydrogen separation ratio (*SR*) into deuterium-protium separation ratio can be done easily with the help of Fenske equation: $SR = \alpha^N$, where N – the number of theoretical plates. A separation factor α is the value of elementary separation effect. It can be presented as a ratio between saturation vapor pressures for pure components. For ortho-para separation it can be shown as: $\alpha_{o-p} = \frac{P_{sat.Para}}{P_{sat.Ortho}}$, where α_{o-p} – ideal separation factor for ortho-para hydrogen system, $P_{sat.Para}$ and $P_{sat.Ortho}$ – saturation vapor pressures above pure para- and orthohydrogen, respectively. Thus, for the deuterium-protium case: $\alpha_{D-H} = \frac{P_{sat.H_2}}{P_{sat.HD}}$, where α_{D-H} – ideal separation factor for system of protium and deutherohydrogen, $P_{sat.H_2}$ and $P_{sat.HD}$ – saturation vapor pressures for pure normal H2 and pure HD, respectively.

Dependencies of separation factors for HD–H_2 and ortho-para hydrogen system on temperature are shown in Fig. 4. The significant difference between the separation factors according to Fenske equation results in much larger difference between the separation ratios for a large number of theoretical plates in the column (or height of the column: *N* = H/HETP). Height Equivalent to a Theoretical Plate (HETP) is the main characteristic of column's performance. The higher separation power corresponds to greater number of theoretical plates (*N*) and less HETP value.

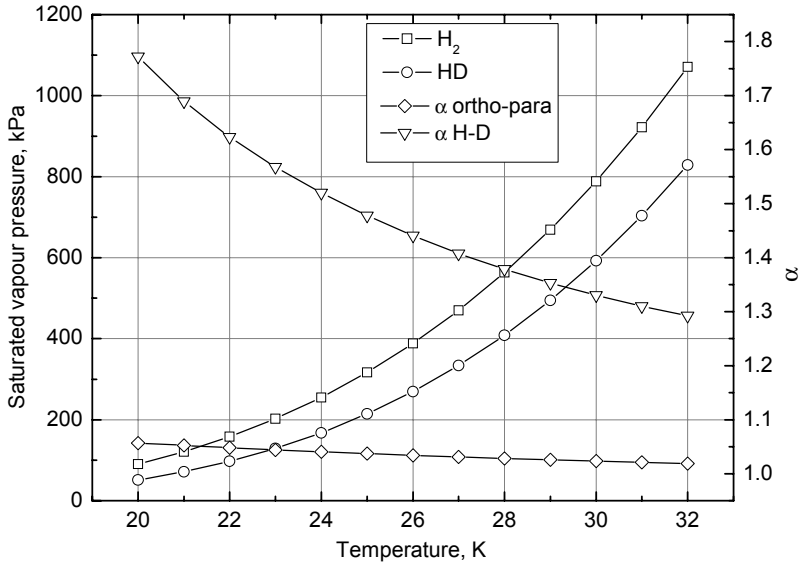

Fig. 4. Temperature dependencies of saturated vapor pressures and separation factors for H_2–HD and ortho- parahydrogen systems

3.2. Results of natural gas separation at total reflux mode

First DRU run was carried out with the natural hydrogen with 126.7 ppm of Deuterium. The column was filled by liquid hydrogen in large excess, and after 1 hour operation excess gas (84 litres) was withdrawn from the column bottom. This explains low final deuterium concentration in the bottom (Table 1). Withdrawn gas was sufficiently enriched to change largely the average concentration in the column. Initial gas volume was 181.6 litres. Negative deuterium concentration in the column top (~1.9 ppm) indicates the accuracy of the measurement. The method consists in extrapolation of sample measurement from deuterium concentration in natural hydrogen and gives low accuracy nearby zero concentration.

Table 1

Natural hydrogen run results

Probe location	**Deuterium, ppm**	**Ortho, %**
Original gas	126.7	75
Column top	–1.9	14.6
Middle	–	32.2
Column bottom	56.2	85
Average concentration calculated from the mass balance	7.7	53.5

The experimental data for the ortho-para separation was fitted by the Fenske equation. The average HETP calculated on the basis of tests with various vapor flow rates was 2.2 cm (Fig. 5), which is comparable with the best results in the world.

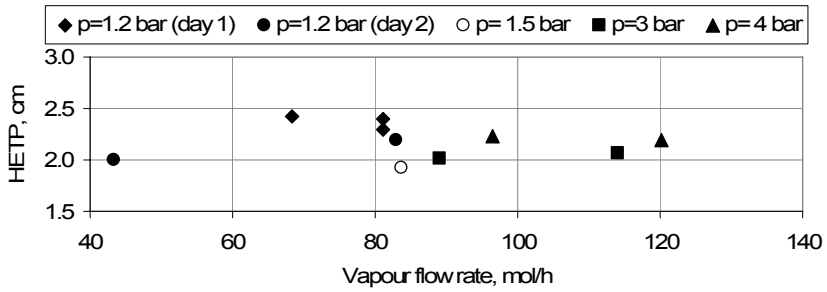

Fig. 5. HETP dependence on vapor flow rate

3.3. Studies on the pressure drop and the liquid holdup

Figure 6 (left) shows the relation between pressure drop across the column and vapor flow rate for the tested mass exchange packing. Unfortunately we did not reach flooding due to relatively large inner column diameter. Original design value was 16 mm, but according to the number of circumstances the inner diameter of 22 mm was chosen, this means that packing was working at relatively low load. We had some anxieties in this respect but fortunately they were relieved due to the excellent packing performance. Packing holdup presented in Fig. 6 (right) had an expected high value. In spite of this the time of reaching a steady state by the column is short – about 1 hour.

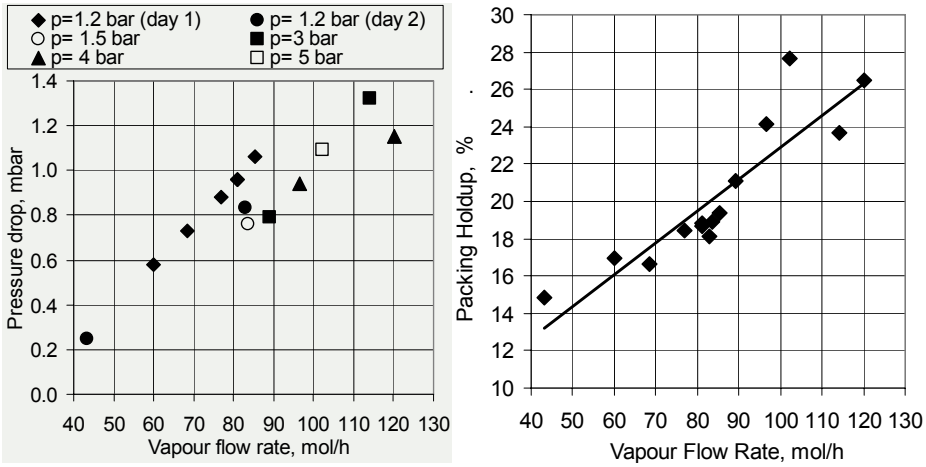

Fig. 6. Pressure drop across the column and packing holdup

3.4. Production of Deuterium Depleted Protium

There are several possible DRU operation modes for the deuterium depleted protium production. Four modes were tested during experiments: “feed through” with purging, “feed through” without purging, continuous circulation through CHUPS and so-called Rayleigh depletion. During the Rayleigh depletion the column was totally flooded by liquefied hydrogen. After the flooding, the hydrogen was discharged through the product line. Natural hydrogen was used only for preliminary tests. The accumulating of required product was carried out from pre-depleted protium. Mass-flow controllers of CHUPS system were used to operate the feed (MFC5) and for the product flow (MFC4). The rate of the purging flow was adjusted by manual needle valve with the help of bubble flow meter. The results of the cleaning runs are shown in the Table 2.

Table 2

Results of the cleaning

Mode		"Feed through" no purging	"Feed through" with purging	Rayleigh's depletion	CHUPS Circulation
Reboiler power, W		20.5	19.0	12.0	20.0
Pressure, bar		1.5	1.5	1.5	2.0
Feed flow, l/min		0.81	0.81	1.25	0.55
Ortho, %	Top	67.8	69.4	-	64.8
	Middle	69.2	74.6	94.2	69.3
	Bottom	96.4	98.5	-	98.2
HD initial, ppm		3	3	10	<3
HD expected, ppm	Top	< 0.01	< 0.01	0.09	< 0.01
	Bottom	123	~ 200	370	-
HD probe		№ 50	№ 57	№ 61	№ 67
Amount of gas, SL		572	630	390	420
Bottom probe HD measured, ppm		57.5 ± 1.2	76.9 ± 1.6	probe lost	16.2 ± 0.5

In addition, a number of deuterium depleted probes were collected (so-called zero protium samples). Expected HD concentrations were calculated using the special program “CD-2004” on the basis of the column’s model with known HETP and total height. The measurements of the probes were performed on the new 200 kV Tandem accelerator built for isotope analysis in Zurich. A special ion source was constructed giving extremely low backgrounds of hydrogen ions from walls, *etc.* The walls are continuously sputtered to keep the background low allowing measurements during 2 hours. The existence of the zero samples from the DRU system turned out to be crucial, since the accelerator gives a different background if the ion source is not fed with hydrogen gas. First zero sample measurement gave zero deuterium concentration at 0.14 ppm sensitivity. Thus, it contains less than 0.14 ppm of deuterium. The difference in expected HD concentration and measurement for probes 50 and 57 is most likely caused by wrong assumption about initial HD concentration, which was measured with extrapolation method and has large error. According to probe 50 measurement, the initial HD concentration should be 1.40 ± 0.03 ppm that corresponds to the initial hydrogen measurement on the accelerator (1.44 ± 0.13 ppm).

Deuterium concentration profile in the column, calculated on the base of the ortho- and para-hydrogen separation, gives very low concentration in the top of the column (Fig. 7). Such a low concentration could not be proved by direct measurement because of relatively low sensitivity of the mass spectroscopy.

The additional direct analysis of zero samples using accelerator mass spectrometry in Zurich gave a better result for depleted hydrogen from the top of the column: less than 60 ppb at 60 ppb sensitivity. This is ten times better than technical requirements of MuCap experiment.

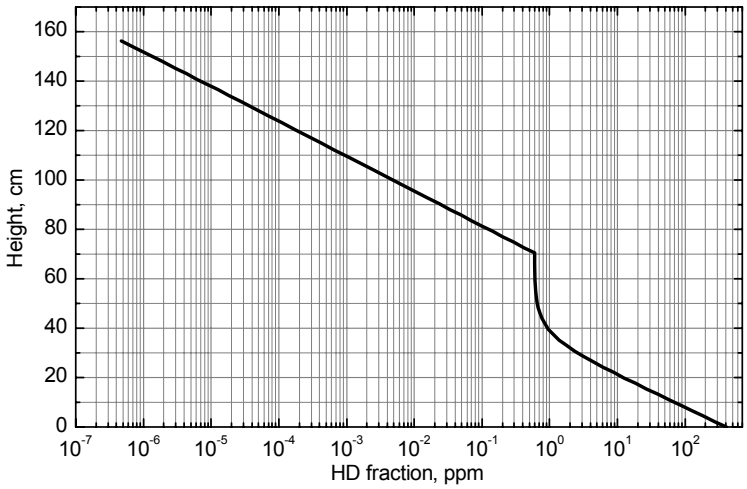

Fig. 7. Expected HD concentration profile. Feed flow = 1 L/min; pressure = 1.5 bar; purging flow = 0.015 L/min; HETP = 2.2 cm; initial deuterium atomic fraction = 3 ppm

4. Conclusion

The Deuterium Removal Unit was designed and manufactured in PNPI during the fall and winter of 2005–2006. The final installation, tests and protium manufacturing were carried out in spring 2006 at the PSI. The separation characteristics of the column were studied in details. Due to the absence of direct prompt method of deuterium measurements, the indirect method of chromatographic analysis for ortho- and para-isomers of hydrogen was used to estimate the column's separation efficiency. Some interesting data were obtained.

The height equivalent to a theoretical plate (HETP) for the column is 2.2 cm. It is one of the best ever obtained results for columns of low and medium cryogenic power. For the present column, HETP value is almost constant in a wide range of vapor flow rate.

The column has the separation power in excess for the goal to be sought. Output deuterium concentration lower than 0.1 ppm almost does not depend on the initial concentration (natural hydrogen can be used!).

The pure orthohydrogen useful for some experimental physics applications can be produced by the setup as well as protium.

After the selection of column's operating parameters and the development of its operating algorithm the protium production run was performed. Several modes of isotope purification were used. As a result about 1.3 m^3 of deuterium depleted hydrogen was obtained. The CHUPS system was put into the mode of continuous hydrogen circulation through the column to remove deuterium.

The productivity of the system in the "feed through" mode is 500 L/day. In the mode of circulation through the CHUPS system it comes to 150 L/day. The mode of Rayleigh depletion is considered to be inefficient because of small initial amount of hydrogen in the column.

The method of measurement of low deuterium content in hydrogen (1 ppm and less) is suggested. It is based on deuterium enrichment by a factor of 40 (and even more) in the reboiler.

This work is also of great importance for Detritiation Plant of PIK reactor as in accordance with a new developing design of the plant the cryogenic column with close parameters is needed. A good packing was developed and tested, successful experience was gained.

References

1. A. Vasilyev, B. Bezymyannykh, V. Ganzha, P. Kravtsov, G. Shapkin, V. Trofimov and M. Vznuzdaev, talk at *the National Hydrogen Association Annual Hydrogen Conference 2005*, Washington, USA.
2. I.A. Alekseev *et al.*, Preprint PNPI-2702, Gatchina, 2006. 26 p.
3. I.A. Alekseev, I.A. Baranov, S.D. Bondarenko, S.N. Chernoby, O.A. Fedorchenko, G.A. Sukhorukova, V.D. Trenin and V.V. Uborski, Fusion Technology **28**, 1579 (1995).

ARCHITECTURE Of SMALL COMPUTING CLUSTERS IN HIGH ENERGY PHYSICS

A.N. Lodkin, A.A. Oreshkin, A.Y. Shevel, T.S. Serebrova

1. Introduction

In last years we see that large **High Energy Physics (HEP)** collaborations use high performance computing clusters. Most of the clusters are integrated into World Grid infrastructure. At the same time, we observe that small clusters do continue to play their own role in the computing life. We mean ***small*** for the cluster up to about 50 machines or so. It is quite obvious that such small cluster is supposed to serve relatively small physics group, may be about 10 physicists. A good time is now to discuss a realistic scenario how physics data might be processed and analyzed and what computing architecture might be used by small physicist's teams.

Contemporary architecture of small computing clusters in **HEP** for physics analysis is based on the commodity hardware. In most of cases it is a Personal Computer (**PC)** based on Intel compliant microprocessors. Scientific Linux is the main operating system. It is better when the computing cluster is a member of a Grid Virtual Organization(s). Here we plan to discuss several aspects of computing cluster design and implementation and how small clusters are related to large computing installations.

2. Large clusters

Several important clusters of Tier 1 & Tier 2 are mentioned in Table 1 (N/A means that the information is *Not Available*). Each cluster of level Tier 1 has tens of **FTEs** in the staff. Most of such clusters have 10 Gbit or more external connectivity. Most of Tier 2 clusters have external channels in between 1 Gbit and 10 Gbit. There are expectations that in 2010 many Tier 1 clusters will have 1 Tbit channels.Each cluster uses a batch system – usually one or two from the range: **LSF**, **Condor**, **Torque**/**PBS**, **SGE**.

Table

Number of hosts and data volumes on several computing clusters in HEP (info from HEPiX October 2006)

Laboratory	**Facility type**	**Number of hosts in clusters**	**Data volume on disks**	**Data volume in Mass Storage**
BNL	Tier 1	~2.0 K	~400 TB	~4.0 PB
Canadian GridX	Tier 1	~1.2 K	~100 TB	~0.4 PB
FNAL Grid Computing Center	Tier 1	~3.0 K	~700 TB	~4.0 PB
GridPP/RAL	Tier 1	~2.9 K	~168 TB	N/A
NIKHEF	Tier 1	~0.3 K	~ 70 TB	N/A
SLAC	Tier 2	~1.7 K	~755 TB	N/A
GRIF(France)	Tier 2	~1.2 K	~700 TB	N/A
INFN	Tier 1	~1.3 K	~600 TB	N/A

Of course clusters are included into one or several Grid Virtual Organizations (**VO**). One of the consequences is that the bulk data moving over World Area Network (**WAN)** must be planned and performed with Grid tools. Each VO has its own rules on the data moving. There is special person (manager) responsible for data moving process. At the same time if the bulk data moving is started it is difficult to predict when the operation would be accomplished. Due to this fact in many large clusters the user jobs are planned to be cancelled if the data requested by jobs are not available in local disk space.

Apparently clusters Tier 1 (or even Tier 2) are main source of physics data and main repository for the software of almost any kind. Often it is required to create new data with special selection algorithm from other data before start an analysis. Because resulted data are peculiar or even private the small physicist's team needs to keep the data in own disk space which could be obtained on large cluster for relatively short period of time. In many cases a small computing cluster is best place to keep own data for long time.

When small physicist's team plans to use existing large cluster it important to know not only power of the cluster but the administrative conditions on the cluster [1,2]. For example if any non privileged user can keep just 40 jobs in the run stage (permitted to use 40 CPUs), it does not matter for him that the cluster consists of 10K machines. Of course in Grid architecture someone can easily send jobs to another cluster where the data are, i.e. it possible to use more than one computing cluster. However in most of real situations some data moving and other additional operations are required. Real advantage to use more than one cluster can be gained if specific conditions are taken place [3]. In this discussion it is assumed that clusters are really stable. The stability in general and difficulty to predict future status of the Grid clusters is a hot topic for now. Anyway, there is an expected advantage with using of two computing clusters instead of one.

3. Estimates for accelerating of computing with two clusters

Let us imagine two clusters where we can do some data analysis or data simulation. For example one cluster is in one research institute and another cluster is in another institute or university, the clusters have independent administration. For simplicity we will use terms *local cluster* and *remote cluster*. We consider the ***computation*** as bunch of simulation (data generation) jobs or data analysis jobs which could be performed on any of two clusters. Usually the bunch of jobs is performing many hours or many days. All jobs are considered as accomplished when the computing itself is ended and the data are moved to final (target) place, for instance to small computing cluster.

Let us introduce several variables:

$\boldsymbol{T}$ – the time for computing task with using one (local) cluster;

$\boldsymbol{\tau}$ – the time for computing with two clusters;

$\boldsymbol{t_l}$ – average time for processing of one portion of the data on one (local) cluster;

$\boldsymbol{t_r}$ – average time for processing of one portion of the data on one (remote) cluster;

$\boldsymbol{t_o}$ – the average overhead time which is required to process one portion of the data on remote cluster; we can include in this time anything we need to make computation possible in remote cluster, for example, time to transfer the data to (from) remote cluster;

$\boldsymbol{D}$ – total number of the data portions which have to be processed;

$\boldsymbol{S}$ – the number of data portions which are processed per time unit;

$\boldsymbol{\alpha}$ – acceleration of the computing due to use of additional cluster.

Now we can write for only (local) cluster $S = \frac{1}{t_l}$ and total time for data processing is

$$T = \frac{D}{S} = D \cdot t_l .$$

For two clusters (local and remote) we can write $S = \frac{1}{t_l} + \frac{1}{t_0 + t_r}$ and total time for the computing is

$$\tau = \frac{D}{\left(\frac{1}{t_l} + \frac{1}{t_0 + t_r} \right)} .$$

It is assumed that the jobs will be sent to remote cluster only when local cluster if fully loaded with our jobs. Now accelerating is

$$\alpha = \frac{T}{\tau} = t_l \cdot \left(\frac{1}{t_l} + \frac{1}{t_0 + t_r} \right) = 1 + \frac{t_l}{t_0 + t_r} .$$

Above might be rewritten as

$$\alpha = \frac{(t_0 / t_r + 1 + t_l / t_r)}{(t_0 / t_r + 1)} .$$

From above formula we see that the accelerating is quite sensitive to the overhead time t_o (please see in Fig. 1) Even in case when remote cluster has huge throughput, when value t_r can be considered close to 0, we have the acceleration is limited by t_o.

It is possible to conclude:

- the expected acceleration for the computing with two clusters can be relatively easy estimated;
- the use of two computing clusters instead one cluster does not mean guaranteed decreasing the computation time in all cases, concrete overheads are very important;
- in long term plan (many days or weeks) the probability that the remote cluster is up and running properly is important.

If we plan to keep the data on small cluster apparently it is more effective to analyze the data on the same cluster.

All above reasons do lead to understanding that in a range of cases the use of small computing cluster is very helpful. Let us consider the architecture of such clusters.

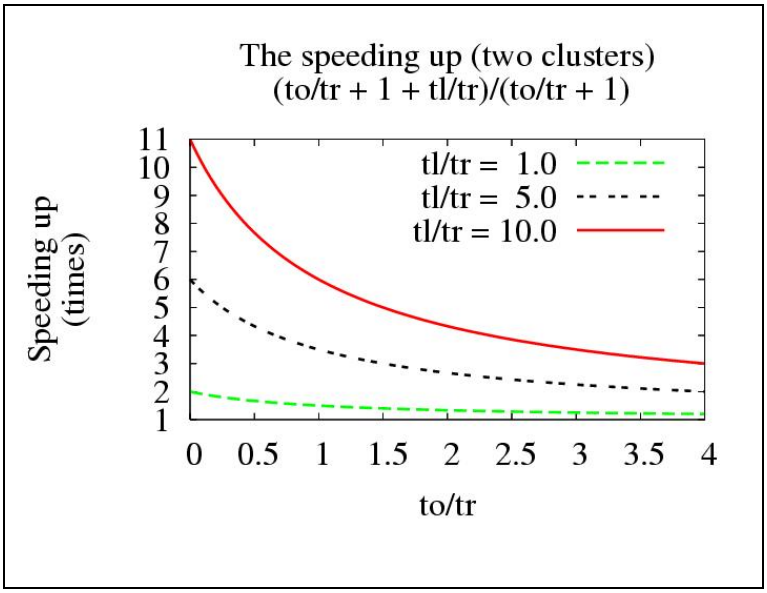

Fig. 1. Computing acceleration with two clusters with different conditions

4. Cluster architecture considerations

Last years **CPU** (microprocessor) performance is increasing at the rate around 60% per year. At the same time disk read/write speed is increasing about 10% per year. Also disk volume per spindle is increasing at the rate around 60% per year. It means that access to disk space (especially in **HEP**, due to extremely large volume of the data) is more and more often becomes a bottleneck. There are many reasons to think that such the relations in between mentioned values will be kept at least for several years in the future.

In the light of such facts and facing the need to analyze tremendous volume of the data the methods how to make read/write operations in parallel are most hot topic. One of the methods is to use advanced **RAID** controllers and advanced cluster file system, for example, **Lustre**, **PVFS**, **GFS**, **GPFS**, **Panasas**, **StorNext**, and the like.

Another very simple method was suggested in the presentation [4]. The approach assumes two opposite configurations and many in between. First is to use one central machine in the cluster where connected all **RAID**s. Opposite configuration is to use the disk space on each machine in the cluster as shown in Fig. 2. Here all file systems are mounted by **NFS** over separate network channel for each file system. More specialized systems like **xrootd** are addressing the same target: to make I/O operation in parallel. Another important point in small cluster is architectural features which permit to reduce the requirements of local maintenance to the minimum.

5. Remote maintenance for small computing cluster

When new cluster design is under consideration we need to take into account the trends with less available manpower in future years. In other words we have to plan as much as minimum local maintenance activity. To permit remote experts to do their job the cluster must be equipped with appropriate components.

Vital and stable solution may be implemented with using the special hardware. We mean type of devices so called **KVM** switch. **KVM** switch (or just **KVM**) is device which connects all control lines (keyboard, mouse, monitor) from each cluster node. **KVM** has connectors to connect real keyboard, monitor, and mouse. Also **KVM** has ability to connect (logically) real keyboard, mice, monitor to any desired server in the cluster.

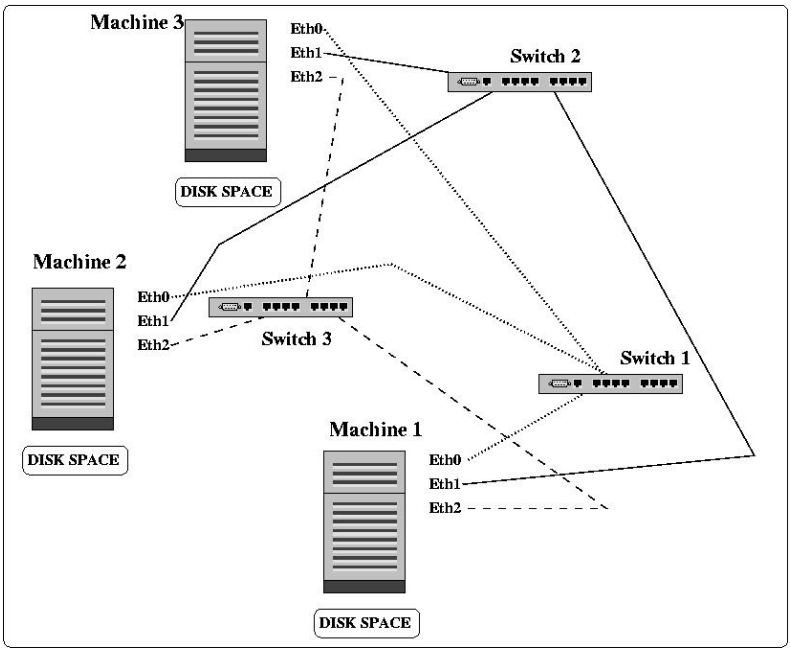

Fig. 2. Cluster scheme where each machine has own disk space

Another device entitled *remote IP console* (**RIPC)** is used as interface in between **KVM** and Internet. An expert on remote computer can use Web browser (with enabled Java functionality) to make connection to the device **RIPC** with protocol **https** and see the screen on **Java** applet. **Java** applet displays redirected console screen, keyboard, and mouse of the cluster where **RIPC** is attached. In other words the expert is able to use local for him keyboard, mouse as they would be attached to the cluster.

Among other mandatory components of the cluster we can mention **UPS** – to make electricity power more stable – and **PDU -** to have ability to switch electrical power **on** and **off** for specified machine in the cluster. An air conditioning is also in range of requirements.

The basic requirements were enumerated. Now other details concerning the software have to be discussed.

6. Technological cluster software and middleware

A range of technological services are seemed very important in contest of easier maintenance procedures. Usually it is very important to have reserve copy of critical data - backup service. Much better is to have reserve copy on the tape cartridges. The tape drive might be used for reserve copy for the physics data as well. Personal subsets of physics data copied on the tape cartridge are often great advantage for physicist.

All cluster users must be in cluster user mailing list. This list is to be used for the information about the changes on the cluster. Such the mailing list may be implemented in several places. One of the useful ways to keep mailing list for small physics team is site http://groups.google.com/.

Cluster administrative system is aimed to deploy, configure and support cluster (to keep all system parameters in consistent state) and is in active use on many clusters. Good examples of such the systems are **OSCAR**, **ROCKS**, and the like.

Batch processing on the cluster is usually performed with one of several batch systems: **Torque/PBS**, **Condor**, **Sun Grid Engine**, **LSF**. Fortunately batch systems in use on large clusters are pretty same as for small clusters. One of the specialized batch tools is **PROOF.** It is the system for users who does like to be all the time inside **ROOT** environment. Part of physicists do use **PROOF** for data analysis.

Monitoring systems are almost same as for large clusters, for instance **Ganglia** and **Nagios.**

Grid middleware is another large software component which is required if the cluster is included into one or more Grid Virtual Organizations. The part of middleware components are the same for all VOs (basic **Globus** toolkit and the like.). A good fraction of middleware is developed by concrete VO and it is not supposed to be used outside the VO.

7. Application software and related databases

Application software dedicated for concrete physics is large fraction of all software tools on the computing cluster. This software has as a rule many versions (may be several tens). Usually people keep all versions on the cluster. Such the software is kept on leading clusters (Tier 1) in **AFS** tree. In general it is possible to use it over **AFS,** however real experience shows that much better to keep local copy of the software. It is performed with one or another set of mirroring mechanisms for example once a week or so. It is quite safe for small physics team especially if some problems are appeared on leading clusters (**AFS** server is down, application software tree becomes unusable). Almost the same we can repeate about such databases as geometry/calibrations database, *etc*.

8. Small cluster support over years

The cluster is running, data analysis is in progress but time is going on and new versions of software (application, system, middleware) are appeared. Quite often you have to do upgrade the software to guarantee that you have same common software packages as your colleagues do. That means somebody has to be careful about consistency of the software.

Furthermore with the time (one, two, three years) you might (very probable) discover that some machines in the cluster are broken or out of date and do not meet newest requirements. Common rule is to remove from the cluster any machine which gives any kind of problems. In average if we like to keep the computing cluster abilities on top – we have to plan to change about 1/3 machines in the cluster every year. It means to remove old machine from cluster and add new machine instead. The machines retired from the cluster might be used as personal machines for students, physicists, *etc*. The reach source of useful information about computing clusters is available at the site http://hepd.pnpi.spb.ru/ClusterGate.RU.

9. Conclusion

Obviously it is not possible to use small computing clusters ***instead of*** large clusters of Tier 1 or 2. It is very useful as a complement to large computing installations; also they make use of large computing facility more optimal. Taking into account that prices for disks and CPUs are going down, it is clear that about 20–50 machines with 50–100 TB of disk space are foreseeable for small physicist's team for most of analysis needs.

References

1. B. Jacak, R. Lacey, S. Mioduszewski, D. Morrison, A. Shevel and I. Sourikova, talk presented at *the Conference on Computing in High Energy Physics CHEP2003* (La Jolla, USA, 24 – 28 March 2003), presentation TUCT009 in http://www.slac.stanford.edu/econf/C0303241/proceedings.html
2. A. Shevel, B. Jacak, R. Lacey *et al.*, in *the Proceedings of the Conference on Ccomputing in High Energy Physics CHEP2004* (Interlaken, Switzerland, 24 September – 1 October 2004), Geneva, 2005. p. 974.
3. A. Shevel and R. Lacey, talk presented at *the Clobus World Conference* (Boston, USA, 7 – 11 February 2005).
4. A. Shevel and R. Lacey, poster presentation at *the Conference on Computing in High Energy Physics CHEP2006* (Mumbai, India, 13 – 17 February 2006).

THIRD GENERATION COORDINATE READOUT SYSTEM – CROS-3

N.F. Bondar, V.L. Golovtsov, A.G. Golyash, E.A. Lobachev, L.N. Uvarov, S.L. Uvarov, V.I. Yatsura

The design and development of the fast and cost effective readout electronics for the tracking detectors is the scope of interest of the modern experiments such as LAND (performed at GSI, Darmstadt), FAMILON, *etc*. The setup of the experiments includes fine pitch MultiWire Proportional Chambers (MWPC) and wire Drift Chambers (DC) with hexagonal cell structure. Variety of modern integrated circuits together with advanced PCB technology allowed to develop the best quality CROS-3 devices and meet the requirements of the experiments.

Block diagram of the CROS-3 system in Fig. 1 includes:

- 96-channel MWPC Digitizers (CDR96);
- 16-channel DC Digitizers (AD16);
- 16-channel Concentrators (CCB16);
- System Buffer (CSB).

Analog part of the CDR96 is based on a CMP_G ASIC performing wire signal amplification and shaping as well as pulse discrimination with peaking time of 30 ns, minimum threshold of 7 fC, double pulse resolution of 80 ns, and power dissipation about 35 mW/channel.

Analog part of the 16-channel DC Digitizer is based on a ASD-Q ASIC [1] with similar functionality and the following characteristics: peaking time of 7 ns, operational threshold at 2–3 fC, double pulse resolution of 20 ns, and power dissipation about 35 mW/channel.

Digital part of either Digitizer is implemented in a Xilinx Spartan-3 FPGA that performs both digitization and readout tasks. Input signals are digitized and delayed to compensate for the trigger latency. Upon receiving a trigger signal, a temporary buffer stores programmable number of time bins. Then the encoder looks for the signal leading edge and encodes both its wire number and its relative time slice number. The delay range compensates trigger latency of up to 2.5 μs in 10 ns steps. The finest time bin resolution is 2.5 ns for the AD16 and 10 ns for the CDR96 cards. Maximim number of time slices is 255 for AD16 and 64 for CDR96. Readout is performed over a STP CAT5 cable at a 100 Mb/sec bit rate.

The CCB16 collects data from up to 16 Digitizers into temporary buffers, which are read out to the CSB via an optical fibre at a 2.0 Gb/sec bit rate.

The CSB is implemented as a universal PCI card.

Figure 2 shows system components mounted directly on the chamber.

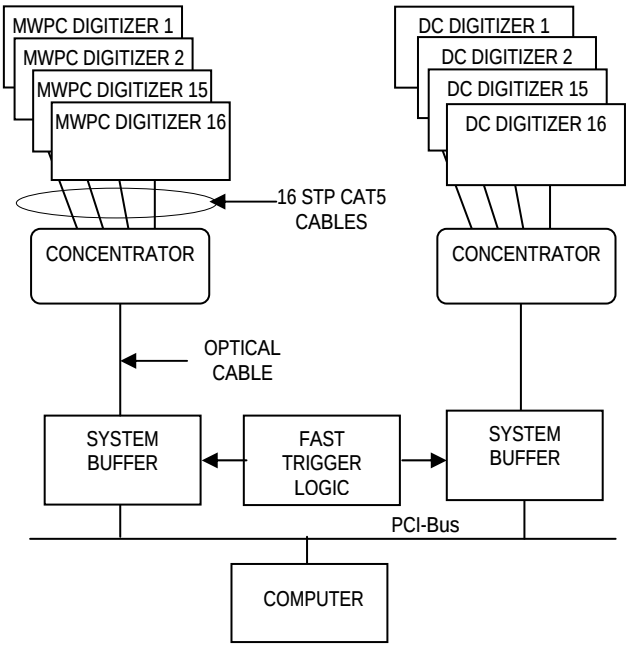

Fig. 1. CROS-3 block diagram

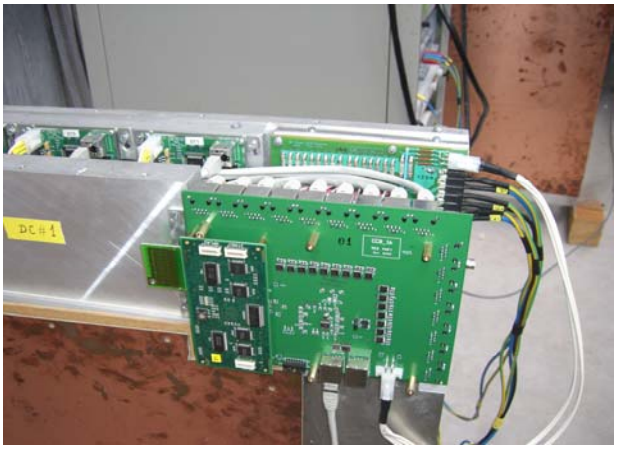

Fig. 2. CROS-3 Digitizers and Concentrator are on-chamber mounted system components

References

1. W. Bokhari *et al.*, CDF/DOC/TRACKING/CDFR/4515 December 1999.

MULTI-CHANNEL HIGH VOLTAGE DISTRIBUTION AND MONITORING SYSTEM FOR LHCb MUON CHAMBERS

S.V. Bondarev, N.B. Isaev, V.I. Lazarev, A.V. Mylnikova, L.O. Sergeev, S.S. Volkov

A multi-channel High Voltage Distribution and Monitoring System (HVDM) was designed and constructed for muon chambers produced at PNPI for the LHCb Muon detector. Two options of the system are developed to be used for the chambers. The first one (HVDM_16) allows linear regulation in each distributed channel in a range of 0-3000 V. The second (HVDM_LHCb) one, being radiation hard, allows linear regulation in each distributed channel only within 1000 V.

HVDM block diagram in Fig.1 includes:

1. 36-channel radiation hard Remote Distributors, performing high voltage fan-out from 1 input to 36 outputs, output voltage regulation within 1000 V in 1 V steps, output voltage measurement with 1 V resolution, and output current measurement with 10 nA resolution in $I < 1\ \mu$A, and 100 nA resolution in $I > 1\ \mu$A range (100 μA max current) for each output. The radiation hardness value is up to 4 krad at 2×10^{12} neutron/cm^2.

2. 8-channel Master Distributor, performing high voltage fan-out from 1 input to 8 outputs, voltage regulation from 0 to 3000 V in 1 V steps, output voltage measurement with 1 V resolution, and output current measurement with better then 100 nA resolution (1.5 mA max output current) for each output.

3. 16-channel Distributors, performing high voltage fan-out from 1 input to 16 outputs, output voltage regulation from 0 to 3000 V in 1 V steps, output voltage measurement with 1 V resolution, and output current measurement with 10 nA resolution in $I < 1\ \mu$A and 100 nA resolution in $I > 1\ \mu$A range (100 μA max current) for each output.

4. Primary High Voltage Power Supply, which can be any industrial rack mounted unit, like Matsusada High Voltage Power Supply, model AV-3*50, whose output regulates in a range from 0 to 3000 V.

5. System Interface/Buffer, providing control and monitoring of the Master and Distributors via the Control/Readout Line. It is implemented as a universal PCI card, compliant to PCI 2.2 specification. Card's buffer memory keeps both voltage setting and actual voltage and current values for each channel.

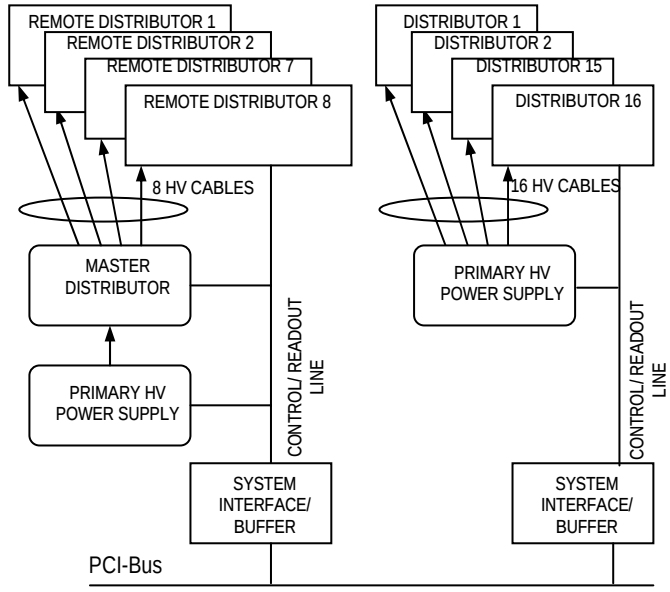

Fig. 1. Block diagram of the HVDM system

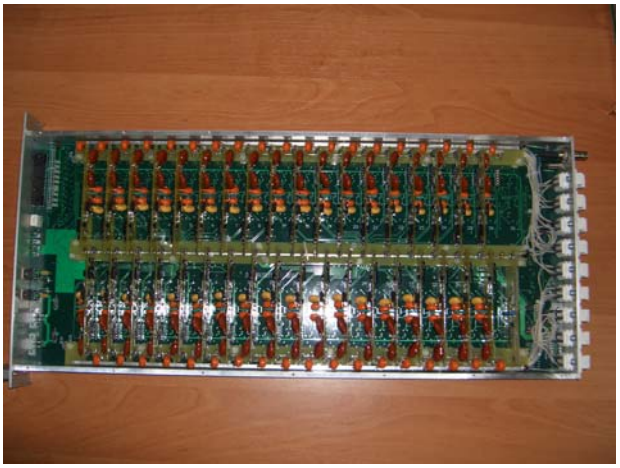

Fig. 2. 36-channel Remote Distributor

The HVDM module dimensions comply with the Eurocard (IEC 297 and IEEE 1101) form factor and are 240 mm × 6U for Master and Distributor, and 540 mm × 6U for Remote Distributor. The HVDM design follows that of the high voltage system developed for the CMS EMU CSC in cooperation with the University of Florida (USA).

Figure 2 illustrates design of 36-channel Remote Distributor with each channel served by a plug-in card.

TRACK FINDING PROCESSOR FOR THE CMS ENDCAP LEVEL 1 MUON TRIGGER

V.L. Golovtsov, L.N. Uvarov, D. Acosta[1)], D. Holmes[1)], K. Kotov[1)], A. Madorsky[1)], S.M. Wang[1)]

[1)] *University of Florida, USA*

A fast three-dimensional Track-Finding Processor was designed for the Level-1 trigger of the CMS endcap muon system. The Track-Finding Processor is implemented as 12 Sector Processors (SP), each of which identifies up to three best muons in a 60-degree azimuthal sector [1]. The purpose of the Track-Finding Processor is to link trigger primitives (track segments) from individual muon stations (four endcap stations ME1-4 and two barrel overlap regions MB1-2) into complete tracks, measure the transverse momentum P_t from the sagitta induced by the magnetic bending, and report the number and quality of tracks to the Level-1 Muon Trigger. The maximum number of track segments collected by one SP is 15 per 25 ns bunch crossing.

Block diagram of the SP logic in Fig. 1 includes:

1. Sector Receiver (SR), which receives local charge track information for 15 muons via optical links. This information is then synchronized and reformatted within the SR (*via* look-up tables) into angular variables for the muons: azimuthal angle φ, local bent angle in φ (φb) and pseudo-rapidity η.

2. Five Extrapolation Units (EU), where all possible pairwise combinations of track segments are tested for consistency with a single track. Each EU takes spatial information from two track segments in different stations and tests if those two segments are compatible with a muon originating from the nominal collision vertex with a curvature consistent with magnetic bending in that region.

3. Three Track Assembly Units (TAU) to examine all outputs of the EUs and determine if any two track segment pairs belong to the same muon. If so, those segment pairs are combined and rank is assigned based on the muon stations involved. For this SP design, stations ME2 and ME3 are the key stations. A valid trigger in the end-cup region must have a hit in one of these two stations. The output of the EUs can be separated into three streams: two for patterns keying off ME2 and ME3 in the end-cup region, and one for pattern keying off ME2 in the end-cup or/and barrel overlap region. Up to three tracks may be found per data stream, nine tracks in total for all three streams.

4. Final Selection Unit, which selects the best three muon candidates. It also features cancellation logic for redundant tracks.

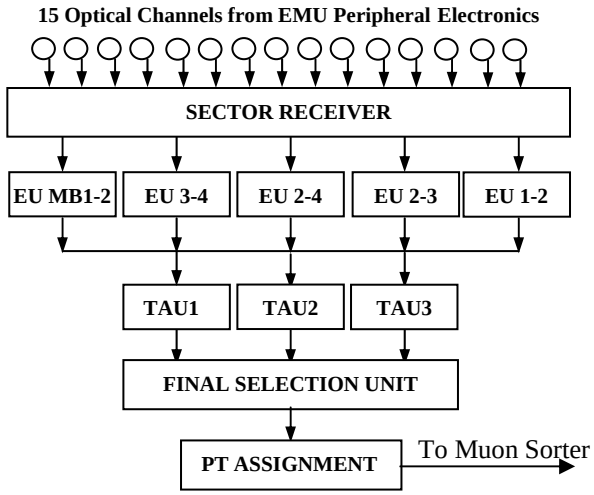

Fig. 1. Sector Processor block diagram

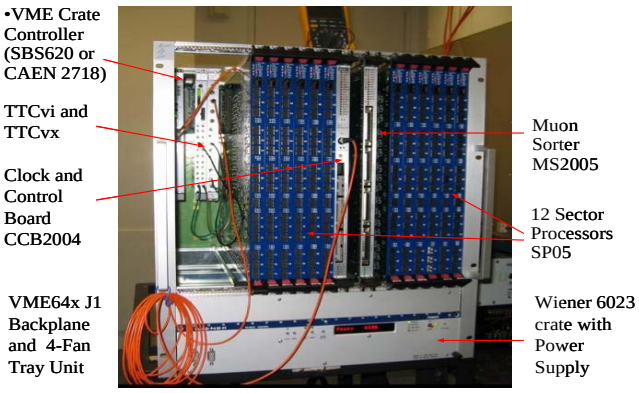

Fig. 2. Track-Finding Crate

5. Assignment Unit, which measures the track parameters of the best three selected muon candidates.

Finally, the best three muon candidates are sent to the Muon Sorter that in turn selects the best four candidates within all tracks of the 12 Sector Processors and sends them to the Global L1 Muon Trigger.

Figure 2 shows a fully assembled Track-Finding Crate with 12 Sector Processors and Muon Sorter.

References

1. D. Acosta *et al.*, Nucl. Instr. Meth. A **496**, 64 (2003).